Asymmetric bistable systems subject to periodic and stochastic forcing in the strongly nonlinear regime: The power spectrum

A. Nikitin* and N. G. Stocks
School of Engineering, University of Warwick, Coventry CV4 7AL, United Kingdom

A. R. Bulsara
Space and Naval Warfare Systems Center D2373, 49590 Lassing Road, San Diego, California 92152-6147, USA

(Received 25 April 2007; published 30 October 2007)

In this, the fourth of a series of papers [the first three papers were Phys. Rev. E **68**, 016103 (2003), **68**, 036133 (2003), and Phys. Lett. A **334**, 12 (2005)] on the response of overdamped noisy bistable systems subject to an asymmetrizing constant signal superimposed on a time-sinusoidal driving signal, we obtain analytic expressions for the power spectral density of the response, including a detailed theoretical analysis of the power spectrum. The results are valid for any two-state system, however the specific case of the Duffing (or standard quartic) potential is considered in detail. The stochastic dynamics are confined to the weak noise limit (periodic signal amplitude much greater than noise intensity), i.e., when the response of the system to the external periodic field is strongly nonlinear.

DOI: 10.1103/PhysRevE.76.041138 PACS number(s): 05.40.−a, 02.50.Ey, 85.25.Dq

I. INTRODUCTION

Periodically driven noisy bistable systems have been extensively studied in the past couple of decades because they are convenient models that can explain some aspects of observed dynamic behavior in real-world nonlinear systems. A good example of such behavior is afforded by the stochastic resonance effect [1] that has been invoked as an explanation of phenomena as diverse as the occurrence of the ice ages [2] and some aspects of neuronal response in the presence of a noise floor [3].

For all its seeming simplicity, however, the dynamics of the model can be very nonlinear, and so an exact analytic solution for the response probability distribution does not exist as yet [4]. Furthermore, in practice, other measures of the response are equally important; for example, in signal processing applications it is the power spectral density (PSD) that is paramount [5] for which exact analytical expressions also do not exist. Approximate treatments (based on a two-state representation of the dynamics or using perturbation theory) have been obtained for the PSD[6–10] but none of these studies consider the case of asymmetry.

The power spectrum of the response of the two-state system contains two components: delta-peaks and a continuous background. The background, for the linear response case of a weak periodic force amplitude and large noise intensity is known to be Lorentzian [6]. In the opposite (nonlinear response) limit of weak noise and a large subthreshold periodic force amplitude, the spectral background has the form associated with an oscillatory output, i.e., the background contains dips that occur near the even multiples of the driving frequency. These dips were observed experimentally [11–13], for the case of *symmetric* bistable systems, predicted theoretically in singular form [14], and described by a phenomenological law [13]. To date, however, the most rigorous theoretical description of the noise background, including the dips, is found in [8]. However, none of these studies have considered the effect of system asymmetry. In practice all physical systems will have a degree of asymmetry and hence it is important to quantify this effect.

The influence of asymmetry on the dynamics of a periodically driven bistable system has received little attention (especially with respect to the PSD) in comparison to the symmetric case, and this provides our goal—to develop a comprehensive theory for the asymmetric bistable system. Our study has both an academic interest as well as potential applications, one application is to the detection of weak dc signals [15,16].

Our approach builds on the method introduced by Stocks [8], which considered a symmetric bistable system. These studies show the consequences of breaking symmetry. This symmetry breaking not only perturbs features in the PSD that exist in the symmetric case but leads also to entirely different phenomenon that can only occur in the asymmetric system; for example, asymmetry-induced peaks were found to occur in the PSD background [17]. Our approach has resulted in a large number of results that have been split into a series of papers [15–17], a brief summary of these papers now follows.

In our first article [15] we found the hierarchy of switch times distributions (between the stable attractors) for the asymmetric bistable system driven by noise $\xi(t)$ with zero mean $\langle \xi(t) \rangle = 0$ and correlation function $\langle \xi(t)\xi(t') \rangle = 2D\delta(t - t')$, and the strong periodic force $A\cos(\Omega t)$:

$$\dot{x} = -\frac{\partial V(x,t)}{\partial x} + \xi(t), \tag{1}$$

where the periodically rocked double-well potential is $V(x,t) = -(a/2)x^2 + (b/4)x^4 + cx - Ax\cos(\Omega t)$. The stochastic equation (1) describes an overdamped particle motion in the bistable potential $V(x,t)$, with the system asymmetry enter-

*Corresponding author.

ing through the parameter c, and the symmetric case corresponding to $c=0$.

Our results [15] are obtained for the following conditions.

(i) The adiabatic regime. In this regime, the periodic force $A\cos\Omega t$ is very slow, i.e., the driving frequency Ω is much less than the relaxation times $\tau_{\mathrm{rel}_1}=[V''_{xx}(x_1,t)]^{-1}$ and $\tau_{\mathrm{rel}_2}=[V''_{xx}(x_2,t)]^{-1}$ of the potential wells where $x_{1,2}$ are the minima of the potential $V(x,t)$.

(ii) Weak noise intensity and strong forcing limit, $A/D \gg 1$, with *subthreshold* amplitude A, i.e., the theory is valid for forcing amplitudes smaller than those required to induce deterministic switching which requires

$$A < \min(A_{c1},A_{c2}),$$

$$A_{ci} = \left| c - (-1)^i \frac{2}{3} a \sqrt{\frac{a}{3b}} \right|, \quad i = 1,2, \tag{2}$$

where A_{c1} and A_{c2} are the critical values of the amplitude corresponding to each potential well (due to a finite c, the wells have unequal depths).

Our analysis of the switch times for the asymmetric bistable system allowed us to find an optimal measurement strategy of weak dc signal detection which we presented in [16].

In the Letter in [17] we reported on peaks in the power spectrum background that only occur in the presence of a symmetry-breaking dc signal. We gave a brief outline of the method of calculation of the PSD background and showed some preliminary analysis of the peaks. In the present paper we show the PSD calculation in detail and obtain an expression for the full power spectrum coupled with a detailed theoretical analysis of its features. More specifically, we present a detailed study of the delta-peaks of the PSD and the spectral background. We also observe dips and peaks in the spectral background and discuss how these are modified and influenced by asymmetry. We note that the results presented are of direct relevance to studies of stochastic resonance and problems of weak magnetic field detection [18,19] and the detection of magnetic fields at nanometer scales [20] via occurrence of even harmonics of the periodic force [21].

II. THE POWER SPECTRUM

For this calculation, we use a procedure that was described in [22] and adapted to the case of a two-state filtered stochastic process driven by a periodic force [8]. Following [8] we invoke the two-state filter

$$y = \begin{cases} 2X: & x > 0, \\ 0: & x < 0, \end{cases} \tag{3}$$

on the system response (here the parameter X is the amplitude of the two-state filter output); this removes all information about intrawell motion, leaving us with a sequence of "spikes" corresponding to excursions across the threshold (the unstable maximum of the potential energy function V). Thus the filter response contains only the switch dynamics that can be described by the master equation,

$$\dot{w}_1 = -[W_{12}(t) + W_{21}(t)]w_1 + W_{21}(t),$$

$$w_1 + w_2 = 1, \tag{4}$$

where w_1, w_2 are the probabilities of being in the states 1 ($y=0$) and 2 ($y=2X$), and $W_{12}(t)$, $W_{21}(t)$ are the transition rates from the states $1\to2$ and $2\to1$, respectively. The rates $W_{12}(t)$ and $W_{21}(t)$ are periodic with period $T=2\pi/\Omega$. In [15] we show that the rates can be approximated by the set of Gaussian peaks

$$W_{12}(t) = \sum_{n=-\infty}^{\infty} W_{12\ \max} \exp\left(- \frac{(t-nT)^2}{2\delta t_1^2} \right) \tag{5}$$

and

$$W_{21}(t) = \sum_{n=-\infty}^{\infty} W_{21\ \max} \exp\left(- \frac{[t-(n+1/2)T]^2}{2\delta t_2^2} \right), \tag{6}$$

with the heights $W_{12\ \max}$ and $W_{21\ \max}$,

$$W_{12\ \max} = \frac{\sqrt{|V''_{xx}[x_1(t'),t']V''_{xx}[x_s(t'),t']|}}{2\pi} \times \exp\left[\frac{V[x_1(t'),t'] - V[x_s(t'),t']}{D} \right], \tag{7}$$

for $t'=0$, and

$$W_{21\ \max} = \frac{\sqrt{|V''_{xx}[x_2(t'),t']V''_{xx}[x_s(t'),t']|}}{2\pi} \times \exp\left[\frac{V[x_2(t'),t'] - V[x_s(t'),t']}{D} \right], \tag{8}$$

for $t'=T/2$, and the widths

$$\delta t_1 = \sqrt{D/|x_1(nT) - x_s(nT)|A\Omega^2} \tag{9}$$

and

$$\delta t_2 = \sqrt{D/|x_2[(n+1/2)T] - x_s[(n+1/2)T]|A\Omega^2}, \tag{10}$$

where n is an integer. Here x_1 and x_2 are the locations of the minima of the potential, and x_s is the location of the maximum between them. The transition rates $W_{12}(t)$ and $W_{12}(t)$ are schematic shown in Fig. 1(a).

The response of the two-state filter is well-represented by the pulse sequence,

$$y(t) = \sum_{n=0}^{\infty} (-1)^n s(t-t_n), \tag{11}$$

where $s(t)=2X\Theta(t)$, t_n is the time at which the nth transitions occurs, and $\Theta(t)$ is the Heaviside function:

$$\Theta(t) = \begin{cases} 0: & t < 0, \\ 1: & t \geqslant 0, \end{cases} \tag{12}$$

with X taken as the amplitude of the two-state filter output.

To calculate the spectral density it is useful to introduce the window function

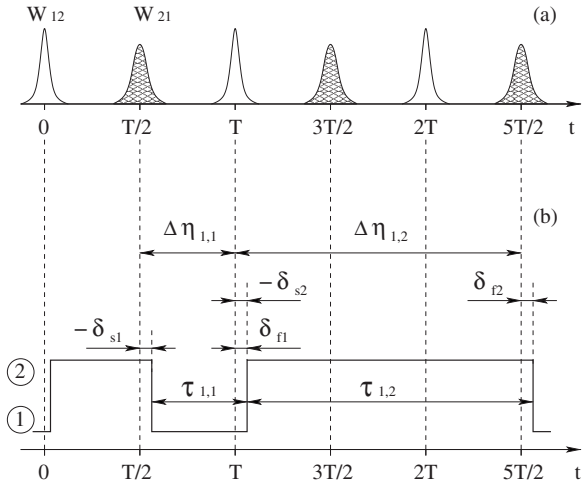

FIG. 1. (a) The transition rates $W_{12}(t)$ and $W_{21}(t)$, and (b) typical response of the two-state filter.

$$\psi_L(t) = \begin{cases} 1: & |t| \leqslant L, \\ 0: & |t| > L. \end{cases} \tag{13}$$

Then the spectral density can be defined as

$$Q(\omega) = \lim_{L\to\infty} \frac{1}{2\pi}\frac{1}{2L}\langle|\hat{y}_L(\omega)|^2\rangle, \tag{14}$$

where the hat denotes the Fourier transform which is taken over an interval of time $2L$,

$$\hat{y}_L(\omega) = \int_{-L}^{L} y(t)\exp(-i\omega t)dt. \tag{15}$$

Since the bistable system (1) is periodically driven, the process $y(t)$ is nonstationary, but, as shown in Appendix A, the definition (14) is equivalent to the power spectrum averaged over an initial phase ϕ of the periodic force, $A\cos(\Omega t+\phi)$, $\phi \in [0:2\pi]$.

The stochastic process $y(t)$ can be rewritten in the form of a convolution integral

$$y_L(t) = \int_{-\infty}^{\infty} \beta_L(t-t')s(t')dt', \tag{16}$$

where

$$\beta_L(t) = \psi_L(t)\sum_{n=0}^{\infty}(-1)^n\delta(t-t_n). \tag{17}$$

Using the convolution theorem, $\hat{y}_L(\omega)=\hat{\beta}_L(\omega)\hat{s}(\omega)$, the PSD can be written as

$$Q(\omega) = \lim_{L\to\infty}\frac{1}{4\pi L}|\hat{s}(\omega)|^2\langle|\hat{\beta}_L(\omega)|^2\rangle, \tag{18}$$

where

$$|\hat{s}(\omega)|^2 = \frac{4X^2}{\omega^2}, \tag{19}$$

and the Fourier transform of $\beta_L(t)$ is

$$\hat{\beta}_L(\omega) = \sum_{n=n_1}^{n_1+N_r-1}(-1)^n\exp(-i\omega t_n), \tag{20}$$

N_r being the number of transitions which occur on the time interval $2L$.

Then, using the expression $(-1)^{n+m}=(-1)^{m-n}(-1)^{2n}=(-1)^{m-n}$, we can write

$$\begin{aligned}|\hat{\beta}_L(\omega)|^2 &= \hat{\beta}_L(\omega)\hat{\beta}_L^*(\omega)\\ &= \sum_{m=n_1}^{n_1+N_r-1}(-1)^m\exp(-i\omega t_m)\sum_{n=n_1}^{n_1+N_r-1}(-1)^n\exp(i\omega t_n)\\ &= \sum_{m=n_1}^{n_1+N_r-1}\sum_{n=n_1}^{n_1+N_r-1}(-1)^{m-n}\exp(-i\omega(t_m-t_n)).\end{aligned} \tag{21}$$

We now introduce the new variable $\tau_{j,n}$ via

$$t_m - t_n = t_{j+n} - t_n = \tau_{j,n},$$

$$j = m - n, \tag{22}$$

so that the expression for $\langle|\hat{\beta}_L(\omega)|^2\rangle$ can be rewritten

$$\begin{aligned}\langle|\hat{\beta}_L(\omega)|^2\rangle &= \left\langle\sum_{j=-N_r+1}^{-1}\sum_{n=n_1-j}^{n_1+N_r-1}(-1)^j\exp(-i\omega\tau_{j,n})\right\rangle\\ &+ \left\langle\sum_{n=n_1}^{n_1+N_r-1}\exp(-i\omega\tau_{0,n})\right\rangle\\ &+ \left\langle\sum_{j=1}^{N_r-1}\sum_{n=n_1}^{n_1+N_r-1-j}(-1)^j\exp(-i\omega\tau_{j,n})\right\rangle.\end{aligned} \tag{23}$$

Assuming N_r to be very large, and since N_r and $\tau_{j,n}$ are almost independent variables, we can average expressions containing N_r and $\tau_{j,n}$ independently, and we can write

$$\begin{aligned}\langle|\hat{\beta}_L(\omega)|^2\rangle &\simeq \sum_{j=-N+1}^{-1}\sum_{n=n_1-j}^{n_1+N-1}(-1)^j\Theta_j(\omega) + \sum_{n=n_1}^{n_1+N-1}\Theta_0(\omega)\\ &+ \sum_{j=1}^{N-1}\sum_{n=n_1}^{n_1+N-1-j}(-1)^j\Theta_j(\omega),\end{aligned} \tag{24}$$

where N is the integer part of $\langle N_r\rangle$ (since N_r is very large we assume $[\langle N_r\rangle - N]/\langle N_r\rangle \simeq 0$), and the characteristic functions $\Theta_j(\omega)$ of the variables $\tau_{j,n}$ are introduced as $\Theta_j(\omega) = \langle\exp(i\omega\tau_{j,n})\rangle$ [23]. Since the characteristic functions are independent from n, we have

$$\langle|\hat{\beta}_L(\omega)|^2\rangle \simeq \sum_{j=-N+1}^{-1}(-1)^j(N+j)\Theta_j(\omega)+N + \sum_{j=1}^{N-1}(-1)^j(N-j)\Theta_j(\omega), \quad (25)$$

where we assume $\Theta_0(\omega)=1$. We also note that $\Theta_{-j}(\omega)=\Theta_j(-\omega)$ as well as the following expression $\Theta_j(-\omega)=\Theta_j^*(\omega)$ is the conjugate of the characteristic functions. Then, we can rewrite Eq. (25) as

$$\langle|\hat{\beta}_L(\omega)|^2\rangle = N+\sum_{j=1}^{N-1}(-1)^j(N-j)[\Theta_j(\omega)+\Theta_j^*(\omega)] = N+2\sum_{j=1}^{N-1}(-1)^j(N-j)\mathrm{Re}\,\Theta_j(\omega). \quad (26)$$

To calculate the power spectrum we need to find the characteristic functions of the random variables $\tau_{j,n}$ contained in Eq. (26). Since the bistable system is asymmetric, we note that the time intervals $\tau_{j,n}$ and $\tau_{j,n+1}$ have different statistics for any number n, but the intervals $\tau_{j,n}$ and $\tau_{j,n+2}$ have identical statistics. This means that we can reduce the number of variables from N into only two: $\tau_{j,1}$ and $\tau_{j,2}$; $\tau_{j,1}$ denotes the interval that started in state 1 (the timing starts when the system first makes a transition to state 1 and stops when it makes a transition to state 2) and similarly $\tau_{j,2}$ is the time interval when the system started in state 2.

Then, the characteristic function $\Theta_j(\omega)$ can be decomposed into two functions

$$\Theta_j(\omega)=\frac{1}{2}C_{j,1}(\omega)+\frac{1}{2}C_{j,2}(\omega), \quad (27)$$

where the indices "1" and "2" of the characteristic functions $C_{j,1}(\omega)$ and $C_{j,2}(\omega)$ denote the starting positions of the pulse sequence (the state 1, or the state 2). Decomposing the summation in Eq. (26) into the summations over odd and even j separately, using Eq. (27), and assuming without loss generality that N is even, we can write

$$\langle|\hat{\beta}_L(\omega)|^2\rangle = N+\sum_{k=1}^{N/2}(N-2k)\mathrm{Re}[C_{2k,1}(\omega)+C_{2k,2}(\omega)] - \sum_{k=0}^{N/2-1}(N-1-2k)\mathrm{Re}[C_{2k+1,1}(\omega)+C_{2k+1,2}(\omega)]. \quad (28)$$

With new definitions of $\tau_{j,1}$ and $\tau_{j,2}$, the variable $\tau_{1,1}$ denotes the time between two transitions when the first transition was to state 1 and $\tau_{1,2}$ denotes the time between two transitions when the first transition was to state 2. These intervals are shown in Fig. 1(b). Clearly, this is a rather complicated way of saying that $\tau_{1,1}$ and $\tau_{1,2}$ are the residence times of states 1 and 2, respectively. The residence times can now be decomposed into a sum of three independent random variables [see Fig. 1(b)],

$$\tau_{1,1}=\Delta\eta_{1,1}+\delta_{s1}+\delta_{f1},$$

$$\tau_{1,2}=\Delta\eta_{1,2}+\delta_{s2}+\delta_{f2}.$$

The variables $\Delta\eta_{1,1}$ and $\Delta\eta_{1,2}$ carry the periodic information and can only take on values of $(m+1/2)T$, $m=0,1,2\ldots$. The variables δ_{s1}, δ_{f1}, δ_{s2}, and δ_{f2} are continuous and take on values $[-T/4:T/4]$. These variables take into account the smearing of the transition point due to noise, i.e., they allow for the fact that the transitions do not occur precisely at integer multiples of $T/2$. The variable δ_{s1} takes into account the smearing when the system makes a transition from state 2 to state 1 (the s denotes that this is the start of the transition sequence) and δ_{f1} takes into account the smearing when the system makes a transition from state 1 to state 2 (the f denotes that this is the finish of the transition sequence). The variables δ_{s2}, and δ_{f2} are the same but for the opposite transition sequence, i.e., the start of the sequence is the transition from state 1 to 2 and the finish of the sequence is the transition from state 2 to 1. Clearly, δ_{s1} and $(-\delta_{f2})$ have identical distributions (i.e., they are i.i.d.) as are δ_{s2} and $(-\delta_{f1})$.

We now consider the calculation of the hierarchy of the characteristic functions with emphasis on the characteristic functions of the residence times and the return times.

In a similar fashion to the residence times, the return time (that is the time required to start from one state and return back again, i.e., the time interval for two transitions) intervals can be decomposed into a set of independent elemental switching events,

$$\tau_{2,1}=\Delta\eta_{1,1}+\Delta\eta_{2,2}+\delta_{s1}+\delta_{f1},$$

$$\tau_{2,2}=\Delta\eta_{1,2}+\Delta\eta_{2,1}+\delta_{s2}+\delta_{f2},$$

where $\Delta\eta_{2,2}$ is the number of periods spent in state 2 and $\Delta\eta_{2,1}$ is the number of periods spent in state 1; again these can only take on values of $(m+1/2)T$, $m=0,1,2\ldots$. We can extend this notation to denote the number of time periods between switching event k and $(k+1)$ as $\Delta\eta_{k,l}$. The $l\in(1,2)$ denotes which state the system was in between the two switching events.

Therefore, for the general case, we have the following decomposition,

$$\tau_{j,1}=\sum_{k=1}^{j}\Delta\eta_{k,[2-(k \bmod 2)]}+\delta_{s1}+\delta_{f[2-(j \bmod 2)]} = \Delta\eta_{1,1}+\Delta\eta_{2,2}+\Delta\eta_{3,1}+\Delta\eta_{4,2}+\cdots+\delta_{s1}+\delta_{f[2-(j \bmod 2)]},$$

which starts from the state 1, and

$$\tau_{j,2}=\sum_{k=1}^{j}\Delta\eta_{k,[1+(k \bmod 2)]}+\delta_{s2}+\delta_{f[1+(j \bmod 2)]} = \Delta\eta_{1,2}+\Delta\eta_{2,1}+\Delta\eta_{3,2}+\Delta\eta_{4,1}+\cdots+\delta_{s2}+\delta_{f[1+(j \bmod 2)]},$$

which starts from the state 2.

Since the switching times $\tau_{j,1}$ and $\tau_{j,2}$ include a sum of independent random variables the characteristic functions, $C_{j,1}(\omega)$ and $C_{j,2}(\omega)$, can be rewritten as following products of the characteristic functions,

$$C_{j,1}(\omega) = C_{\Delta\eta_{1,1}}(\omega)C_{\Delta\eta_{2,2}}(\omega)C_{\Delta\eta_{3,1}}(\omega)C_{\Delta\eta_{4,2}}(\omega) \times \cdots \times C_{\delta_{s1}}(\omega)C_{\delta_{f[2-(j \bmod 2)]}}(\omega) \tag{29}$$

and

$$C_{j,2}(\omega) = C_{\Delta\eta_{1,2}}(\omega)C_{\Delta\eta_{2,1}}(\omega)C_{\Delta\eta_{3,2}}(\omega)C_{\Delta\eta_{4,1}}(\omega) \times \cdots \times C_{\delta_{s2}}(\omega)C_{\delta_{f[1+(j \bmod 2)]}}(\omega), \tag{30}$$

where $C_{\Delta\eta_{k,l}}(\omega)=\langle\exp(i\omega\Delta\eta_{k,l})\rangle$, $C_{\delta_{sl}}(\omega)=\langle\exp(i\omega\delta_{sl})\rangle$, and $C_{\delta_{fl}}(\omega)=\langle\exp(i\omega\delta_{fl})\rangle$, $l\in\{1,2\}$. Since all variables $\Delta\eta_{k,1}$ are identically distributed, as are all the variables $\Delta\eta_{k,2}$, we can write $C_{\Delta\eta_{k,1}}=C_{\Delta\eta_{1,1}}$ and $C_{\Delta\eta_{k,2}}=C_{\Delta\eta_{1,2}}$ (see Ref. [15]).

The characteristic functions $C_{j,1}(\omega)$ and $C_{j,2}(\omega)$ have already been found in Ref. [15] and will be used in what follows.

In [15] we find that the distributions of the variables $\delta_{s,fi}$ ($i\in\{1,2\}$) are well approximated by Gaussian functions,

$$P_{\delta_{s,fl}}(\delta_{s,fl}) = \frac{1}{\sqrt{2\pi\sigma_{s,f}^2}}\exp\left(-\frac{(\delta_{s,fl}-\delta_{s,flm})^2}{2\sigma_{s,f}^2}\right), \tag{31}$$

for which the characteristic function is

$$C_{\delta_{s,fl}}(\omega) = \exp(i\omega\delta_{s,flm})\exp\left(-\frac{\omega^2\sigma_{s,fl}^2}{2}\right). \tag{32}$$

Here, we have denoted averaged quantities by $\delta_{s,flm}=\langle\delta_{s,fl}\rangle$, and the dispersions by $\sigma_{s,fl}^2=\langle(\delta_{s,fl}-\langle\delta_{s,fl}\rangle)^2\rangle$. The identity of the distributions $P_{\delta_{s1}}(\delta_{s1})=P_{\delta_{f2}}(-\delta_{s1})$ and $P_{\delta_{s2}}(\delta_{s2})=P_{\delta_{f1}}(-\delta_{s2})$ leads to the identity of the standard deviations $\sigma_{s1}=\sigma_{f2}$ and $\sigma_{s2}=\sigma_{f1}$.

Using short designations $C_{\Delta\eta_{1,2}}(\omega)=\hat{P}$ and $C_{\Delta\eta_{1,1}}(\omega)=\hat{P}'$ for convenience, and also utilizing the equation

$$\sum_{m=0}^{M} a^m = (1-a^{M+1})/(1-a),$$

and the properties of the characteristic functions (see [15]) $C_{\delta_{s1}}(\omega)=C_{\delta_{f2}}^*(\omega)$, and $C_{\delta_{s2}}(\omega)=C_{\delta_{f1}}^*(\omega)$, we can rewrite the expression (28),

$$\begin{aligned}\langle|\hat{\beta}_L(\omega)|^2\rangle = N &+ \mathrm{Re}\left\{N(C_{\delta_{f1}}C_{\delta_{f1}}^* + C_{\delta_{f2}}C_{\delta_{f2}}^*)\frac{\hat{P}\hat{P}'}{1-\hat{P}\hat{P}'}\right\} \\ &- 2\,\mathrm{Re}\left\{(C_{\delta_{f1}}C_{\delta_{f1}}^* + C_{\delta_{f2}}C_{\delta_{f2}}^*)\hat{P}\hat{P}'\frac{1-(\hat{P}\hat{P}')^{N/2}}{(1-\hat{P}\hat{P}')^2}\right\} \\ &- \mathrm{Re}\left\{(N-1)C_{\delta_{f2}}C_{\delta_{f1}}^*\frac{\hat{P}}{1-\hat{P}\hat{P}'}\right\} \\ &+ 2\,\mathrm{Re}\left\{C_{\delta_{f2}}C_{\delta_{f1}}^*\hat{P}^2\hat{P}'\frac{1-(\hat{P}\hat{P}')^{N/2}}{(1-\hat{P}\hat{P}')^2}\right\} \\ &- \mathrm{Re}\left\{(N-1)C_{\delta_{f1}}C_{\delta_{f2}}^*\frac{\hat{P}'}{1-\hat{P}\hat{P}'}\right\} \\ &+ 2\,\mathrm{Re}\left\{C_{\delta_{f1}}C_{\delta_{f2}}^*\hat{P}\hat{P}'^2\frac{1-(\hat{P}\hat{P}')^{N/2}}{(1-\hat{P}\hat{P}')^2}\right\}.\end{aligned} \tag{33}$$

The last expression includes elements proportional to $[1-(\hat{P}\hat{P}')^{N/2}]/(1-\hat{P}\hat{P}')^2$. These elements yield Dirac delta functions in the power spectrum in the limit $N\to\infty$. The elements proportional $1/(1-\hat{P}\hat{P}')$ give the background in the power spectrum.

To calculate the power spectrum, as defined in Eq. (18), we need a representation for the time interval $2L$. It is easily seen that, in the limit of large L, the time interval can by approximated as

$$\begin{aligned}2L &= \frac{N}{2}\langle\tau_{1,1}\rangle + \frac{N}{2}\langle\tau_{1,2}\rangle \\ &= \frac{N}{2}(\langle\Delta\eta_{1,1}\rangle + \langle\delta_{s1}\rangle + \langle\delta_{f1}\rangle) + \frac{N}{2}(\langle\Delta\eta_{1,2}\rangle + \langle\delta_{s2}\rangle + \langle\delta_{f2}\rangle) \\ &= \frac{N}{2}(\langle\Delta\eta_{1,1}\rangle + \langle\Delta\eta_{1,2}\rangle).\end{aligned} \tag{34}$$

The average values $\langle\Delta\eta_{1,1}\rangle$ and $\langle\Delta\eta_{1,2}\rangle$ can be calculated via the following characteristic functions

$$\hat{P}(\omega) = \frac{1}{\cos\frac{\omega T}{2} - i\alpha_q\sin\frac{\omega T}{2}},$$

$$\hat{P}'(\omega) = \frac{1}{\cos\frac{\omega T}{2} - i\alpha_p\sin\frac{\omega T}{2}}, \tag{35}$$

which are found in [15], leading to

$$\langle\Delta\eta_{1,1}\rangle = -i\left.\frac{dC_{\Delta\eta_{1,1}}(\omega)}{d\omega}\right|_{\omega=0} = \alpha_p\frac{T}{2},$$

$$\langle\Delta\eta_{1,2}\rangle = -i\left.\frac{dC_{\Delta\eta_{1,2}}(\omega)}{d\omega}\right|_{\omega=0} = \alpha_q\frac{T}{2}.$$

Finally, the time interval is

$$2L = \frac{N}{2}(\alpha_p+\alpha_q)\frac{T}{2}.$$

The parameters α_p and α_q are the mean times $\langle\Delta\eta_{1,1}\rangle$ and $\langle\Delta\eta_{1,2}\rangle$ measured in units of the half period $T/2$. The α_p and α_q can be defined as

$$\alpha_p = \frac{1+p}{1-p}, \quad \alpha_q = \frac{1+q}{1-q}.$$

The parameters p and q are the probabilities of remaining in states 1 or 2 in the period T. They can be found as solutions of Eq. (4) with the approximations (5) and (6) of the rates. We find $p=\exp(-\sqrt{2\pi}W_{12\,\max}\delta t_1)$ and $q=\exp(-\sqrt{2\pi}W_{21\,\max}\delta t_2)$.

Then, using Eq. (33), the background in the power spectrum can be written as

$$Q_b(\omega) = \lim_{N\to\infty} \frac{2}{\pi T(\alpha_p+\alpha_q)} \frac{4X^2}{\omega^2} \times \left[1 + 2\,\mathrm{Re}\left\{ (C_{\delta_{f1}} C^*_{\delta_{f1}} + C_{\delta_{f2}} C^*_{\delta_{f2}}) \frac{\hat{P}\hat{P}'}{1-\hat{P}\hat{P}'} - C_{\delta_{f2}} C^*_{\delta_{f1}} \frac{\hat{P}}{1-\hat{P}\hat{P}'} - C_{\delta_{f1}} C^*_{\delta_{f2}} \frac{\hat{P}'}{1-\hat{P}\hat{P}'} \right\} \right]. \quad (36)$$

Finally, using Eqs. (35) and (32) the spectral background in the $N\to\infty$ limit can be written as

$$Q_b(\omega) = \frac{8X^2}{\pi T(\alpha_p+\alpha_q)\omega^2} \left[1 - K^{-1} \left\{ [\exp(-\omega^2\sigma_{f1}^2) + \exp(-\omega^2\sigma_{f2}^2)](1+\alpha_p\alpha_q) - \exp\left(-\frac{\omega^2}{2}(\sigma_{f1}^2+\sigma_{f2}^2)\right)\cos(\omega(\delta_{f1m}-\delta_{f2m}))\cos\frac{\omega T}{2}[2(1+\alpha_p\alpha_q)-(\alpha_p+\alpha_q)^2] + \exp\left(-\frac{\omega^2}{2}(\sigma_{f1}^2+\sigma_{f2}^2)\right)\sin(\omega(\delta_{f1m}-\delta_{f2m}))\sin\frac{\omega T}{2}(\alpha_p-\alpha_q)(1+\alpha_p\alpha_q) \right\} \right], \quad (37)$$

where

$$K = (1+\alpha_p\alpha_q)^2 \sin^2\frac{\omega T}{2} + (\alpha_p+\alpha_q)^2\cos^2\frac{\omega T}{2}. \quad (38)$$

The peaks of the power spectrum can be found by using expression (33):

$$Q_p(\omega) = \lim_{N\to\infty} \frac{2}{\pi T(\alpha_p+\alpha_q)} \frac{4X^2}{\omega^2} \left[-\frac{2}{N}\,\mathrm{Re}\left\{ [C_{\delta_{f1}} C^*_{\delta_{f1}} + C_{\delta_{f2}} C^*_{\delta_{f2}}]\hat{P}\hat{P}' \frac{1-(\hat{P}\hat{P}')^{N/2}}{(1-\hat{P}\hat{P}')^2} \right\} + \frac{2}{N}\,\mathrm{Re}\left\{ C_{\delta_{f2}} C^*_{\delta_{f1}} \hat{P}^2\hat{P}' \frac{1-(\hat{P}\hat{P}')^{N/2}}{(1-\hat{P}\hat{P}')^2} \right\} + \frac{2}{N}\,\mathrm{Re}\left\{ C_{\delta_{f1}} C^*_{\delta_{f2}} \hat{P}\hat{P}'^2 \frac{1-(\hat{P}\hat{P}')^{N/2}}{(1-\hat{P}\hat{P}')^2} \right\} \right] \quad (39)$$

which, in the $N\to\infty$ limit, leads to

$$Q_p(\omega) = \frac{8X^2}{\pi} \frac{\left(\alpha_q\frac{T}{2} - \delta_{f1m} + \delta_{f2m}\right)^2}{(\alpha_p+\alpha_q)^2T^2}\delta(\omega) + \sum_{n=-\infty, n\neq 0}^{\infty} \delta(\omega - n\Omega)\frac{4X^2}{\pi^2(\alpha_p+\alpha_q)^2n^2} \times \left[\exp(-\omega^2\sigma_{f1}^2) + \exp(-\omega^2\sigma_{f2}^2) + (-1)^{n+1}2\exp\left(-\frac{\omega^2}{2}(\sigma_{f1}^2+\sigma_{f2}^2)\right)\cos(\omega(\delta_{f1m}-\delta_{f2m})) \right], \quad (40)$$

where $\delta(\cdot)$ is the Dirac function. Clearly, the $Q_p(\omega)$ can be represented as

$$Q_p(\omega) = \sum_{n=-\infty}^{\infty} Q_n\delta(\omega - n\Omega),$$

where Q_n is the power of the nth peak.

Finally, we sum Eqs. (37) and (40) to obtain the complete expression for the power spectrum

$$Q(\omega) = Q_b(\omega) + Q_p(\omega). \quad (41)$$

III. RESULTS AND DISCUSSION

In this section we present a detailed study of the power spectral density (PSD) of the bistable system (1) with the two-state filter, Eq. (3). Equations (37) and (40) are the main results of this paper.

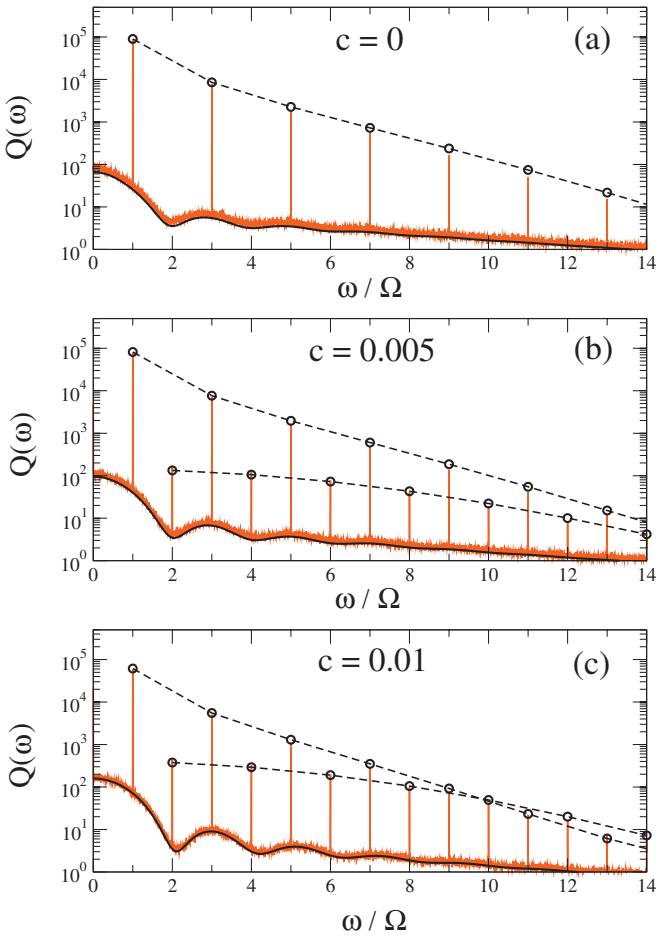

FIG. 2. (Color) The power spectral density (PSD) for parameters (a) $X=1.0$, $a=1.0$, $b=1.0$, $A=0.34$, $D=0.0039$, $\Omega=0.001$, $c=0$, (b) $c=0.005$, and (c) $c=0.01$. The theoretical results are shown by the black lines for the backgrounds and black circles for the peaks. The results calculated by computer simulation are shown by the red lines.

In the symmetric case ($c=0$) Eqs. (37) and (40) simplify to

$$Q_b(\omega) = \frac{4X^2}{\pi T \alpha_p \omega^2} \frac{(\alpha_p^2 - 1)\sin^2(\omega T/4) + 1 - \exp(-\omega^2 \sigma_{f1}^2)}{1 + (\alpha_p^2 - 1)\sin^2(\omega T/4)} \tag{42}$$

and

$$Q_p(\omega) = \sum_{n=-\infty}^{\infty} \frac{4X^2}{\pi^2 \alpha_p^2 (2n+1)^2} \exp(-(2n+1)^2 \Omega^2 \sigma_{f1}^2) \times \delta(\omega - (2n+1)\Omega), \tag{43}$$

where, due to symmetry considerations, the following pairs of parameters are equal: $\alpha_p = \alpha_q$, $\sigma_{f1}^2 = \sigma_{f2}^2$, and $\delta_{f1m} = \delta_{f2m}$. These expressions agree with those obtained by Stocks [8] and, thus, confirm the validity of the calculation.

Theoretical and experimental (i.e., numerically obtained by Monte Carlo simulation) PSDs are shown in Fig. 2 for different values of the asymmetry, c. The agreement between the theoretical PSDs and their numerically obtained counterparts is excellent, this further validates our results. Further discussion of the structure of the PSDs will now concentrate on the behavior of the background and the delta peaks separately.

A. Delta peaks of the power spectrum

An analysis of Eq. (40) shows that, in contrast to the symmetric case, Eq. (43), Eq. (40) contains the oscillating function, $\cos(\omega(\delta_{f1m} - \delta_{f2m}))$, whose period in the frequency domain is $2\pi/(\delta_{f1m} - \delta_{f2m}) \gg \Omega$. It is easy to see that the period becomes infinite when the system is symmetric, since we have $\delta_{f1m} = \delta_{f2m}$ in this case. In the asymmetric case, the period is finite and the peak heights of the harmonics not only decrease with growing number, n, but also oscillate. Moreover, the oscillations of the peak heights for odd and even harmonics are in opposite phases: In the low frequency domain the odd harmonics are more powerful than the even harmonics; the reverse is true in the high frequency domain (see Fig. 2 in which the envelopes of the odd and even harmonics are shown by the dashed lines).

To further analyze the delta-peak components of the PSD it is useful to consider Eq. (40) in the limit of weak noise intensity. Then the parameters σ_{f1}, σ_{f2}, and $(\delta_{f1} - \delta_{f2})$ are vanishingly small [15]. Using the Taylor series representations $\cos(\kappa) \simeq 1 - \kappa^2$ and $\exp(\kappa) \simeq 1 + \kappa$, we obtain the approximations for the strengths of the odd and even harmonics,

$$Q_n \simeq \frac{8X^2}{n^2} \frac{f_{\text{av}}^2}{\Omega^2} [2 - n^2 \Omega^2 (\sigma_{f1}^2 + \sigma_{f2}^2)], \tag{44}$$

where $n \in (1, 3, 5, \ldots)$, and

$$Q_n \simeq 2X^2 f_{\text{av}}^2 (\delta_{f1} - \delta_{f2})^2 [2 - n^2 \Omega^2 (\sigma_{f1}^2 + \sigma_{f2}^2)], \tag{45}$$

where $n \in (2, 4, 6, \ldots)$. Here, the inequality $n^2 \Omega^2 (\sigma_{f1}^2 + \sigma_{f2}^2) \ll 1$ is used (see Appendix D), and the average switch frequency, $f_{\text{av}} = 2/(\alpha_p + \alpha_q)T$, is introduced. The latter quantity can be defined, via the average period T_{av} (the average return time, see [15]), as $f_{\text{av}} = T_{\text{av}}^{-1}$. In turn, the average period T_{av} can be represented as the sum $T_{\text{av}} = \langle \tau_{r1} \rangle + \langle \tau_{r2} \rangle$, where $\langle \tau_{r1} \rangle$ and $\langle \tau_{r2} \rangle$ are the average residence times [15].

Equation (44) shows that the power of the odd harmonics, Q_n, decreases as n^{-2} (the same behavior was recently observed in an experiment [24]). In contrast to the odd harmonics, the even harmonics are only weakly dependent on n [see Eq. (45)] and, hence, their power varies slowly over a wide range of n. Since the power in the even harmonics is proportional to $(\delta_{f1} - \delta_{f2})^2$ they are weak in comparison to the odd harmonics at small n, and disappear altogether in the symmetric case, $c=0$.

Equations (44) and (45) lead to an estimation of the number n at which the peak height envelopes, corresponding to the odd and even harmonics cross [this is evident in Fig. 2(c)]:

$$n_{\text{cross}} \simeq \frac{2}{\Omega |\delta_{f1} - \delta_{f2}|}. \tag{46}$$

i.e., $n_{\text{cross}} \propto |\delta_{f1} - \delta_{f2}|^{-1}$.

Now, for weak noise intensity and weak asymmetry, we have shown [15]

$$\delta_{f1m} \simeq -W_{12\,\max}\delta t_1^2 = -\frac{\sqrt{|V''_{xx}(x'_1,t')V''_{xx}(x'_{s1},t')|}}{2\pi}\exp\left(-\frac{\Delta V_1}{D}\right)\frac{D}{|\Delta x_1|A\Omega^2} \simeq -b_0 D\exp\left(-\frac{\Delta U_0}{D}\right)\left(1-\frac{\Delta x_0 c}{D}\right), \quad (47)$$

where $b_0=\sqrt{|V''_{xx}(x'_1,t')V''_{xx}(x'_{s1},t')|}/(2\pi|\Delta x_0|A\Omega^2)$. Hence the difference $(\delta_{f1m}-\delta_{f2m})$ is

$$\delta_{f1m}-\delta_{f2m} \simeq b_0\exp\left(-\frac{\Delta U_0}{D}\right)2\Delta x_0 c, \quad (48)$$

i.e., the difference is proportional to c and depends exponentially on the noise intensity. This immediately leads to the result $n_{\text{cross}} \propto c^{-1}$.

When $n=1$, the term $n^2\Omega^2(\sigma_{f1}^2+\sigma_{f2}^2)$ of Eq. (44) is sufficiently smaller than 2 that it can be neglected. In this case we obtain the following simple expression

$$Q_1 \simeq 16X^2\frac{f_{\text{av}}^2}{\Omega^2}. \quad (49)$$

Hence the dependencies of the power of the first harmonic Q_1 on the parameters D and c is governed by the dependencies of the square of the normalized average switch frequency f_{av}^2/Ω^2, i.e., Q_1 decreases with increasing asymmetry and Q_1 increases with the noise intensity up to a saturation value [see Figs. 3(a) and 4(a)]. The saturation value is approximately obtained when $2\pi f_{\text{av}}=\Omega$, i.e., when the system is fully synchronized to the periodic drive and, hence, is switching every half period (note that full synchronization cannot happen for all values of c). The experimental dependence Q_1 on the noise intensity has a weak discernible maximum [see Fig. 3(a)]. Further, it is seen [Fig. 3(a)] that the dependencies on D for the higher odd harmonics show a more prominent maxima than that of the first harmonic. The even harmonics have a more prominent maxima in the Q_n versus D curves than the odd harmonics; this is true for results obtained via computer simulations as well as theoretically [see Fig. 3(b)].

In contrast to the dependence of the odd harmonics on the asymmetry c, the dependence of the even harmonics has a maximum—this is shown in Fig. 4. The power of the even harmonic Q_n is proportional to $(\delta_{f1m}-\delta_{f2m})^2$ and f_{av}^2 [see Eq. (45)]. Also, the difference $|\delta_{f1m}-\delta_{f2m}|$ increases with the asymmetry [see Eq. (48)], and the average switch frequency f_{av}^2 decreases with increasing asymmetry. The interplay of these processes leads to the non-monotonic dependence of the power, for the even harmonics Q_n, on the asymmetry c.

B. Spectral background

Examples of the spectral background are shown in Figs. 5 and 6. Clearly the most significant feature is the oscillatory nature of the background. At small noise intensities these oscillations take the form of discrete peaks and dips—the peaks occur at approximately odd integer multiples of the driving frequency and the dips occur at even multiples. As the noise intensity is increased the peaks and dips broaden until eventually they disappear. Physically, the oscillations (i.e., dips and peaks) occur only when the system is *not* fully synchronized to the periodic driving, i.e., when the system is not switching approximately every $T/2$ periods. The origin of the dips and peaks will be discussed in more detail later, first we discuss their structure.

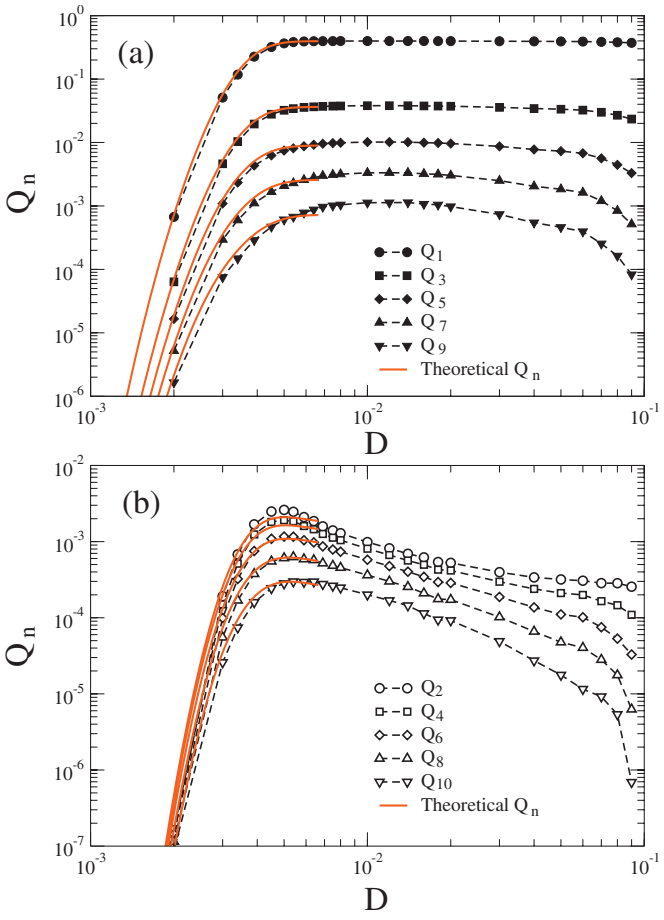

FIG. 3. (Color) Dependence of Q_n on the noise intensity D. Figure (a) corresponds to the odd harmonics and (b) corresponds to even harmonics. The theoretical results [obtained via expressions (40)] are shown by the red solid curves, and the results obtained via numerical simulations of the original system are denoted by symbols (the black dashed lines are guides to the eye). The parameters are $A=0.34$, $\Omega=0.001$, $X=1.0$, $a=1.0$, $b=1.0$, and $c=0.1$.

1. Dips in the background of the power spectrum

For weak noise intensity D (see Fig. 5) the background component of the spectrum has an oscillatory form: It contains dips that occur near even multiples of the driving frequency Ω. The dips can be characterized by their width, depth, and the location of their minima. To estimate the depth of the dips it is useful to introduce the average spectral background,

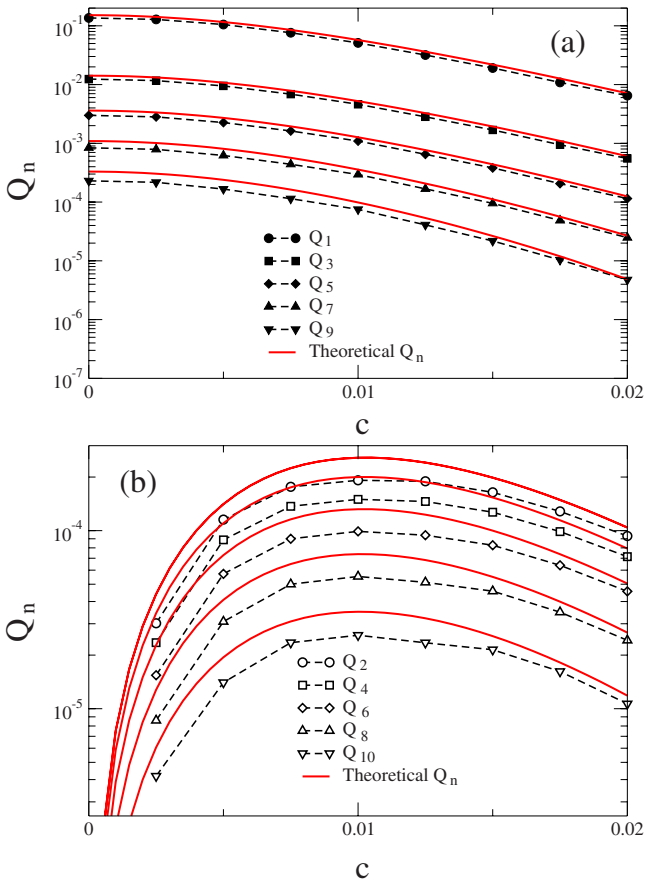

FIG. 4. (Color online) Dependence of Q_n on asymmetry c. Figure (a) corresponds to the odd harmonics and (b) corresponds to even harmonics. The theoretical results [obtained via expressions (40)] are shown by the red solid curves, and the results obtained via numerical simulations are denoted by symbols (the black dashed lines are guides to the eye). The parameters are $A=0.34$, $\Omega=0.001$, $X=1.0$, $a=1.0$, $b=1.0$, and $D=0.003$.

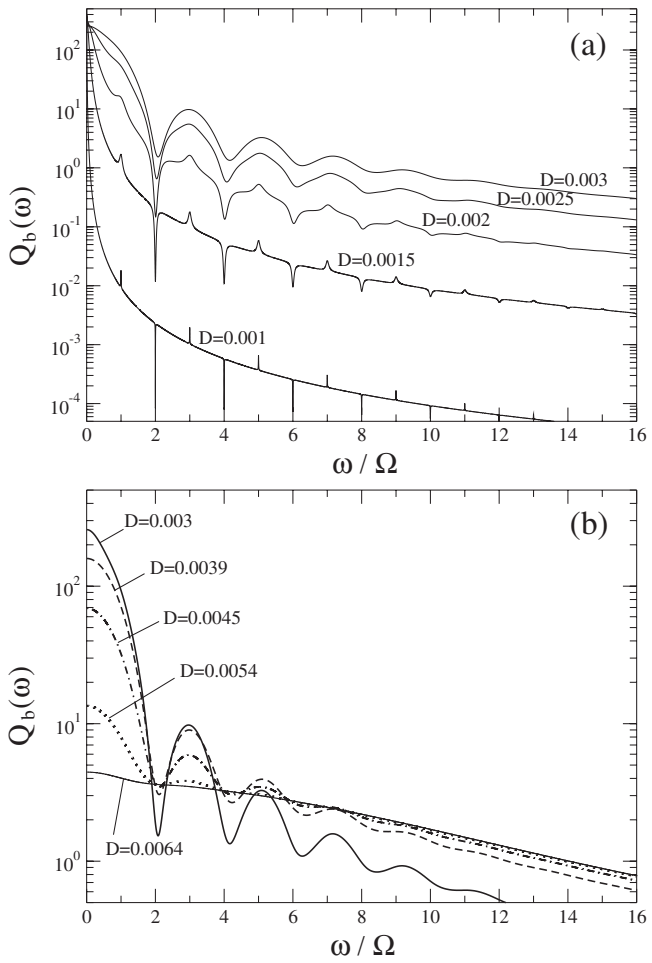

FIG. 5. The background of the power spectrum. Figure (a) is plotted for weak noise intensities, $D\in[0.001:0.003]$, and (b) is plotted for larger noise intensities, $D\in[0.003:0.0064]$. The parameters are $X=1.0$, $a=1.0$, $b=1.0$, $A=0.34$, $\Omega=0.001$, and $c=0.01$.

$$Q_{\mathrm{av}}(\omega)=\frac{8X^2}{\pi T(\alpha_p+\alpha_q)\omega^2}, \tag{50}$$

which can be obtained by removing all the components, that are relevant to the oscillation properties of the background, from Eq. (37). The approximation (50) is shown by the dashed line in Fig. 6(a). It is easy to see that the approximation (50) is a good estimate of the average of the spectral background. As shown in Appendix A, in the weak noise limit the sum $(\alpha_p+\alpha_q)$ is proportional to Ω, i.e., T^{-1} and the expression (50) becomes independent of the driving frequency Ω. Equation (50) shows that, on average, the spectral background of the symmetric system decays (in the weak noise limit) according to the simple law, const$\times\omega^{-2}$. These conclusions, for the asymmetric system under consideration here, are in good agreement with the corresponding conclusions obtained [14] for the symmetric system.

Now, the depth of the dips can be introduced as the difference,

$$d=Q_{\mathrm{av}}(\omega_{\min})-Q_b(\omega_{\min}), \tag{51}$$

where $\omega_{\min}$ is the frequency of the dip minimum. The dependence of the depth d of the first dip on the asymmetry c is shown by the solid lines in Fig. 7(a). It was obtained by using Eq. (37) for which the minimum $\omega_{\min}$ was evaluated numerically. The resulting $\omega_{\min}$ vs c behavior is shown in Fig. 7(b) by the solid lines.

The quantity $\omega_{\min}$ can be replaced by the sum of the frequency $n\Omega$, near which the dip is located, and the shift $\Delta\omega_{\min}$, which is less than the driving frequency, $\Delta\omega_{\min}<\Omega$, i.e., the frequency of the dip minimum is $\omega_{\min}=n\Omega+\Delta\omega_{\min}$. To analyze this shift, the parabolic approximation of the background near its minimum is used,

$$Q_b(\omega)=A_0+A_1(\omega-n\Omega)+A_2(\omega-n\Omega)^2, \tag{52}$$

where the parameters A_0, A_1, and A_2 are defined in Appendix C. The parabolic approximation is shown in the inset of Fig. 6(a), and gives following expression of the shift of the background minima (see Appendix C):

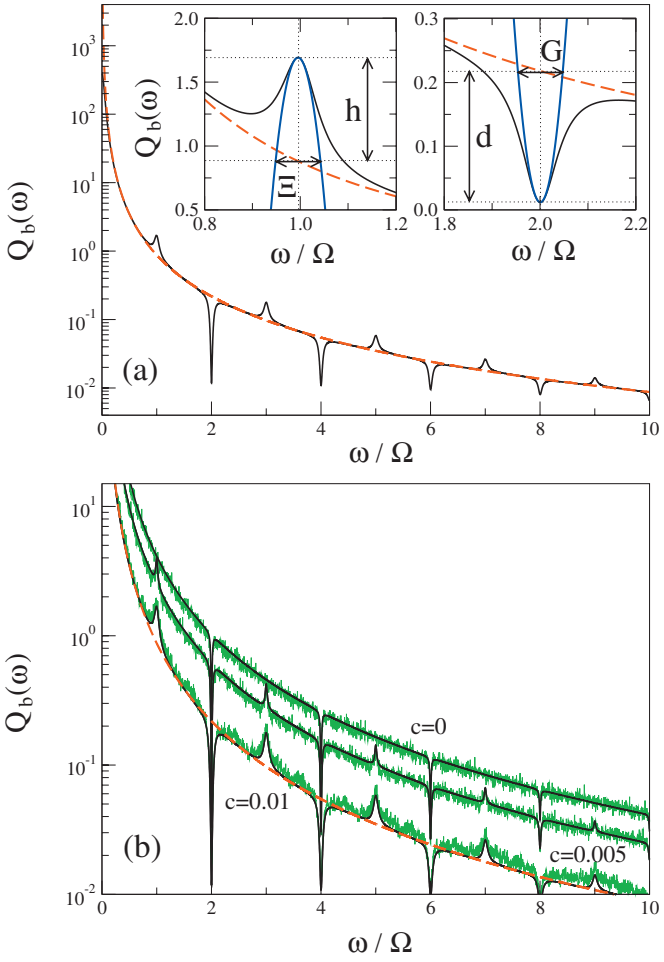

FIG. 6. (Color) (a) The background contribution to the power spectrum for noise intensity $D=0.0015$ and asymmetry $c=0.01$. The solid black line shows the theoretical result obtained from Eq. (37), and the dashed red line represents the approximation of the background by the simple law ω^{-2} [see Eq. (50)]. The parabolic approximations are illustrated in the windows of (a). (b) The background contribution to the power spectrum. The jagged green line shows the result (via computer simulations) from which the periodic components are removed, and the theoretical results are shown by smooth black lines. The dashed red line represents the approximation of the background by the simple law ω^{-2} [see Eq. (50)]. The parameters are $X=1.0$, $a=1.0$, $b=1.0$, $A=0.34$, $\Omega=0.001$, and $D=0.0015$.

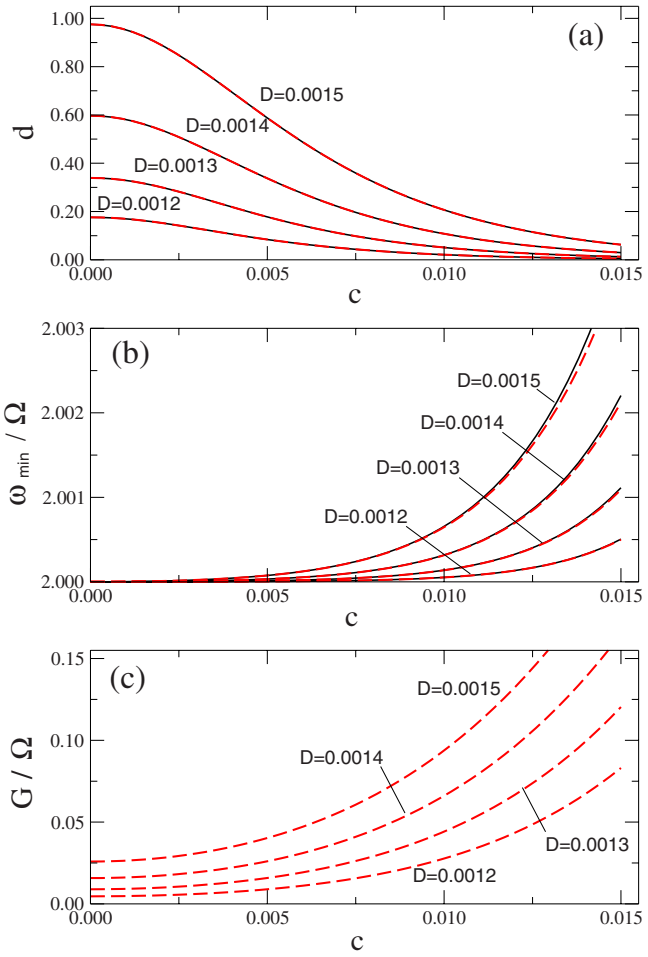

FIG. 7. (Color online) (a) The depth d, (b) the frequency $\omega_{\min}$ of the minimum, and (c) the width G, of the first dip of the spectral background vs the asymmetry c. The results obtained via the expression (37) are shown by solid black lines. The approximate solutions (53), (56), and (59) are shown by dashed red lines. The parameters are $A=0.34$, $\Omega=0.001$, $X=1.0$, $a=1.0$, and $b=1.0$, and the noise intensities $D=0.0015$, 0.0014, 0.0013, and 0.0012.

$$\Delta\omega_{\min} = \omega_{\min} - n\Omega = \frac{n\Omega^2}{2\pi}\frac{(\alpha_p - \alpha_q)(\delta_{f1m} - \delta_{f2m})}{\alpha_p \alpha_q}. \quad (53)$$

Equation (53) shows that the shift is proportional to the difference $(\delta_{f1m}-\delta_{f2m})$ and also the difference $(\alpha_p-\alpha_q)$. We can write the following obvious equation

$$(\alpha_p - \alpha_q) = \frac{2}{T}\left(\alpha_p \frac{T}{2} - \alpha_q \frac{T}{2}\right)$$

$$= \frac{2}{T}(\langle \Delta\eta_1 \rangle - \langle \Delta\eta_2 \rangle)$$

$$\simeq \frac{2}{T}(\langle \tau_{1,1} \rangle - \langle \tau_{1,2} \rangle), \quad (54)$$

which is valid for weak noise intensity only. Equation (54) implies that the shift is proportional to the difference of the residence times. In turn, this difference has been shown [15,16] to be proportional to $D^{-3/2}\exp(\Delta U_0/D)$ and c [see also Eq. (B4)], where ΔU_0 is the potential barrier height in the symmetric case, i.e., when $c=0$.

Then, collecting the results (B2), (B3), and (48), we obtain

$$\Delta\omega_{\min} \simeq d_0 \frac{c^2}{\sqrt{D}} \exp\left(-\frac{2\Delta U_0}{D}\right), \quad (55)$$

where d_0 is given by Eq. (C14), i.e., the shift $\Delta\omega_{\min}$ is proportional to the square of the asymmetry c, and increases with the noise intensity D. Let us note that for large noise intensities the expression (55) describes the nonmonotonical dependence of the shift on D, however, it is incorrect (see Fig. 8), since we are only using the weak noise intensity in Eq. (55). Figure 8 illustrates the dependence of the shift

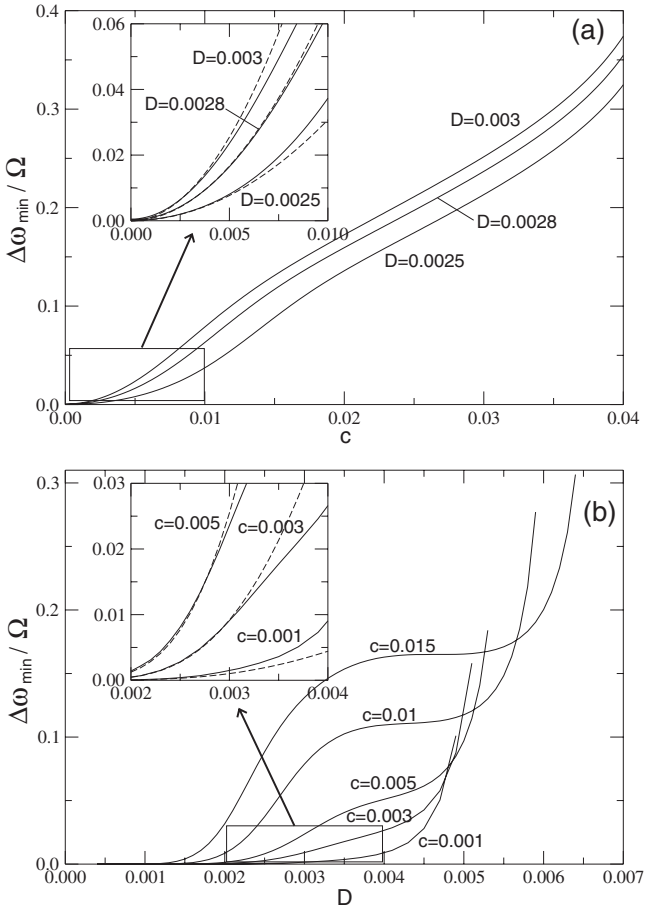

FIG. 8. (a) Shift of the first minimum of the power spectrum background as a function of c and (b) as a function of D. The results obtained by using Eq. (37) are showed by solid lines. The simplified solutions (55) are shown by dashed lines. In the insets we show expanded segments of the results for better viewing. The parameters are $A=0.34$, $\Omega=0.001$, $X=1.0$, $a=1.0$, and $b=1.0$.

$\Delta\omega_{\min}$ on the parameters c and D; the approximate results obtained via Eq. (55) are shown in the insets of this figure. We see that the shifts obtained using Eqs. (37) and (55) are in good agreement for weak noise intensity and asymmetry. Note that the shift occurs to the right, i.e., $\Delta\omega_{\min} \geqslant 0$ for any value of the asymmetry and noise intensity.

The parabolic approximation to the background lets us estimate the width G of the dips. We approach this estimate via the width of the paraboloid on the average background level $Q_{\rm av}(\omega_{\min})$ [see the inset of Fig. 6(a)]. The width of the paraboloid can be found from the equation $Q_{\rm av}(\omega_{\min}) = Q_b(\omega)$, where $Q_b(\omega)$ is the parabolic approximation to the background. It is easy to see that, for weak c and D, the shift satisfies the inequality $\Delta\omega_{\min} \ll \Omega$ so that we can approximately write down $Q_{\rm av}(\omega_{\min}) = Q_{\rm av}(n\Omega + \Delta\omega_{\min}) \simeq Q_{\rm av}(n\Omega)$. Then the solution of the equation $Q_{\rm av}(n\Omega) = Q_b(\omega)$ is

$$\omega_{1,2} = \omega_{\min} \pm \frac{\Omega}{\pi}\frac{\alpha_p + \alpha_q}{\alpha_p \alpha_q},$$

and the width G is expressed as

$$G = 2\frac{\Omega}{\pi}\frac{\alpha_p + \alpha_q}{\alpha_p \alpha_q}. \tag{56}$$

From Eqs. (B1), (B3), and (B5), the dependence of the width G on the weak parameters c and D (for the condition $|\Delta x_0 c/D| \ll 1$) can be found in the form $G \propto \sqrt{D}\exp(-\Delta U_0/D)[1+(\Delta x_0 c/D)^2]$, which shows that the width G increases with the asymmetry and the noise intensity. This conclusion is confirmed by Fig. 7(c) where the results obtained from Eq. (56) are shown by the dashed lines.

As remarked earlier, the oscillatory form of the spectral background occurs at weak noise intensity. In turn, this means that the escape times from the potential wells are much longer than the period of the applied force, i.e., $\alpha_p \gg 1$ and $\alpha_q \gg 1$, and $(1+\alpha_p\alpha_q) \simeq \alpha_p\alpha_q$. It is easy to check that, in the low frequency limit (we can verify this over the frequency range $0 < \omega < 5\ \Omega$), the inequality $\omega^2(\sigma_{f1}^2 + \sigma_{f2}^2) \ll 1$ is true, and the approximations $\exp(-\omega^2(\sigma_{f1}^2+\sigma_{f2}^2)/2) \simeq 1-\omega^2(\sigma_{f1}^2+\sigma_{f2}^2)/2$, $\exp(-\omega^2\sigma_{f1}^2) \simeq 1-\omega^2\sigma_{f1}^2$, and $\exp(-\omega^2\sigma_{f2}^2) \simeq 1-\omega^2\sigma_{f2}^2$ are valid. Then the power spectral density of the background can be rewritten as

$$\begin{aligned} Q_b(\omega) \simeq & \frac{8X^2}{\pi T(\alpha_p+\alpha_q)\omega^2} \\ & \times \Bigg[1 - \frac{[1-\omega^2(\sigma_{f1}^2+\sigma_{f2}^2)/2]}{\alpha_p^2\alpha_q^2\sin^2(\omega T/2) + (\alpha_p+\alpha_q)^2\cos^2(\omega T/2)} \\ & \times \{2\alpha_p\alpha_q + (\alpha_p^2+\alpha_q^2)\cos(\omega T/2) \\ & + (\alpha_q-\alpha_p)\alpha_p\alpha_q\omega(\delta_{f1m}-\delta_{f2m})\sin(\omega T/2)\} \Bigg]. \end{aligned} \tag{57}$$

Comparing Eqs. (53) and (56), it is easy to find that $\Delta\omega_{\min} \ll G$. This means that the approximation $Q_b(\omega_{\min}) \simeq Q_b(n\Omega)$, where $n=2,4,\ldots$, can be used for the estimation of the level of the minima (i.e., the ordinate of their location) and the depth of dips. The equations $\sin(\omega T/2)=0$ and $\cos(\omega T/2)=1$ correspond to this approximation. The level of the minima in the low frequency limit can be obtained from Eq. (57). It is

$$Q_b(n\Omega) = \frac{4X^2}{\pi T(\alpha_p+\alpha_q)}(\sigma_{f1}^2+\sigma_{f2}^2). \tag{58}$$

The expression (58) is independent of n, i.e., the number of the dip. Equation (58) shows that the level of the background minima is proportional to the sum of the dispersions σ_{f1}^2 and σ_{f2}^2, i.e., *the depth of the dips is bordered by the phenomenon of the smearing of the transition times due to noise*. We note that the same conclusion was stated in [13], but only as a hypothesis, which has been, rigorously, confirmed in the present work.

Finally, the estimate of the depth d of the dips can be found as the difference of the average background $Q_{\rm av}(n\Omega)$ and the level of the minima $Q_b(n\Omega)$:

$$d = Q_{\mathrm{av}}(n\Omega) - Q_b(n\Omega) = \frac{4X^2}{\pi T(\alpha_p + \alpha_q)}\left[\frac{2}{n^2\Omega^2} - (\sigma_{f1}^2 + \sigma_{f2}^2)\right], \tag{59}$$

where n is even. From Eq. (59) it follows that the depth d decreases with increasing n. The results obtained by using Eq. (59) are shown in Fig. 7(a) by the dashed lines and compared with the results of Eq. (51). We observe good agreement between Eq. (51) and its estimate Eq. (59).

2. Peaks in the spectral background

From Fig. 6 it can be seen that the spectral background also contains peaks positioned approximately at odd integer multiples of the forcing frequency (we discussed the peaks of the spectral background in [17]). The peaks only occur in the asymmetric case, $c \neq 0$. Each peak can be characterized by the height h, the width Ξ and the location of the maxima $\omega_{\max}$ on the frequency axis. The height of the peak can be introduced as

$$h = Q_b(\omega_{\max}) - Q_{\mathrm{av}}(\omega_{\max}). \tag{60}$$

The height and location of the first peak, obtained numerically from Eq. (37), are shown by the solid lines in Figs. 9(a) and 9(b). We note that the shift ω_{shift} of the peak maximum from the nearest frequency $n\Omega$, defined as $\omega_{\mathrm{shift}} = \omega_{\max} - n\Omega$, is negligible ($\omega_{\mathrm{shift}} \ll \Omega$). This enables us to redefine the peak height as

$$h = Q_b(n\Omega) - Q_{\mathrm{av}}(n\Omega), \tag{61}$$

where n is an odd integer. This expression is useful for calculating the peak heights when the spectral background is obtained numerically using the fast Fourier transform (FFT). The results for the peak height, obtained numerically, are shown in Fig. 9(a) as circles.

It is easy to check that, in the low frequency limit [see Eq. (57)], the height h of the peaks corresponding to the frequency $n\Omega$ can be found as

$$h \simeq \frac{8X^2}{\pi T(\alpha_p + \alpha_q)n^2\Omega^2}\left(1 - \frac{n^2\Omega^2}{2}(\sigma_{f1}^2 + \sigma_{f2}^2)\right)\frac{(\alpha_p - \alpha_q)^2}{(\alpha_p + \alpha_q)^2}. \tag{62}$$

This predicts that the height h of the peaks is proportional to n^{-2}, i.e., it decreases with increasing peak number.

The locations, $\omega_{\max}$, of the peaks occur at, approximately, $(2m+1)\Omega$ where $(m = 0, 1, \ldots)$. However, these maxima are shifted to lower frequency with increasing asymmetry [see Fig. 9(b)]. To analyze this shift we use the parabolic approximation of Eq. (37) near the maxima in the low frequency and weak noise limits:

$$Q_b(\omega) \simeq B_0 + B_1(\omega - n\Omega) + B_2(\omega - n\Omega)^2, \tag{63}$$

where $|\omega - n\Omega| \ll \Omega$, and we have introduced the parameters $B_0 = K_1(1 + K_3K_7)$, $B_1 = -K_1(K_2K_3K_7 + K_2)$, and $B_2 = -K_1K_3K_4K_7$, where K_1, K_2, K_3 and K_4 are introduced in Appendix C, and $K_7 = (\alpha_p - \alpha_q)^2$.

The location of the maxima $\omega_{\max}$ can be found from the equation $dQ_b(\omega)/d\omega = 0$, which for the parabolic approximation (63) has the solution

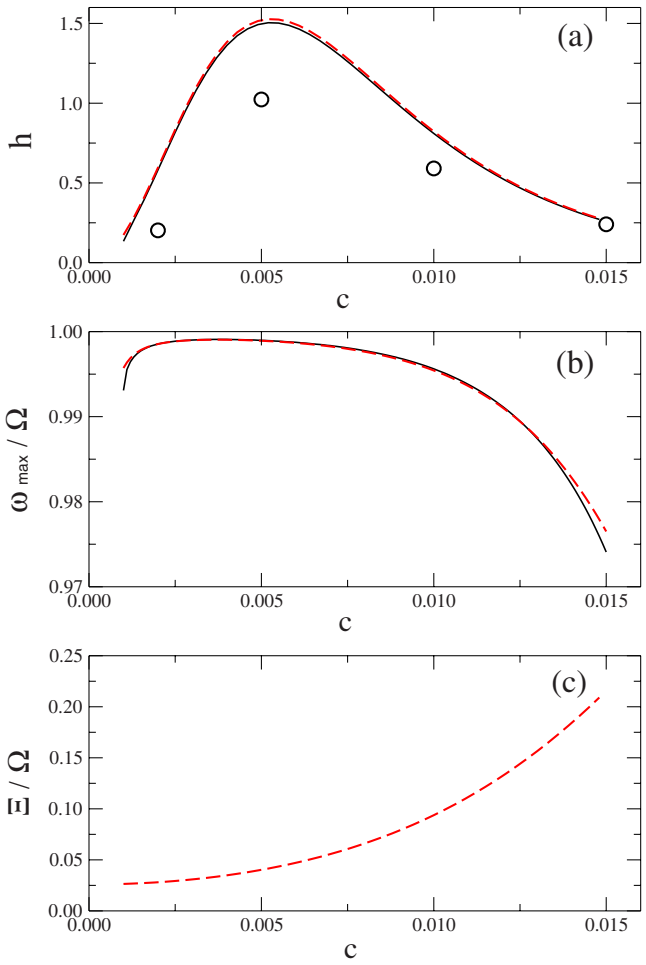

FIG. 9. (Color online) (a) Height h as a function of the asymmetry c. (b) Frequency $\omega_{\max}$ of the first maximum of the spectral background vs c. (c) Width of the peaks vs c. The height and location of the first peak, obtained numerically from Eq. (37), are shown by the solid black lines in figures (a) and (b). The circular data points are from digital simulation. The approximations for h, $\omega_{\max}$, and Ξ given by Eqs. (62), (64), and (65), respectively, are shown by the red dashed lines. The parameters are $X = 1.0$, $a = 1.0$, $b = 1.0$, $A = 0.34$, $D = 0.0015$, and $\Omega = 0.001$.

$$\omega_{\max} = n\Omega - \frac{\Omega}{n\pi^2}\frac{(\alpha_p + \alpha_q)^2}{\alpha_p^2\alpha_q^2} \times\left(1 + \frac{1}{1 - (n^2/2)\Omega^2(\sigma_{f1}^2 + \sigma_{f2}^2)}\frac{(\alpha_p + \alpha_q)^2}{(\alpha_p - \alpha_q)^2}\right). \tag{64}$$

Equation (64) shows that the shift ω_{shift} of the maxima occurs to the left ($\omega_{\mathrm{shift}} < 0$) and is proportional to n^{-1}, i.e., it decreases with increasing peak number. The shift of the spectral peaks has a non-monotonic dependence on the asymmetry c [see Fig. 9(b)], i.e., there is a value of the asymmetry c^* when the shift from the nearest frequency $n\Omega$ is minimal.

The parabolic approximation of the background enables us estimate the width Ξ of the peaks. We approach this estimate (analogous to the procedure employed for the dips)

via the width of the paraboloid on the average background level $Q_{\mathrm{av}}(\omega_{\max})$ [see inset in Fig. 6(a)]. The width of the paraboloid can be found from Eqs. (50) and (63) as the solution of the equation $Q_b(\omega)=Q_{\mathrm{av}}(\omega_{\max})$. However, a simpler solution can be found by assuming that $\omega_{\max}\simeq n\Omega$ and $Q_{\mathrm{av}}(\omega_{\max})\simeq Q_{\mathrm{av}}(n\Omega)$. This gives

$$\Xi = 2\frac{\Omega}{\pi}\frac{\alpha_p+\alpha_q}{\alpha_p\alpha_q}. \tag{65}$$

It is easy to see that Eqs. (56) and (65) are the same, i.e., the widths of the peaks and the widths of the dips are identical. The approximations for h, $\omega_{\max}$ and Ξ given by Eqs. (62), (64), and (65), respectively, are shown in Fig. 9 by the dashed lines.

3. Regime of synchronized switching

The expression (37) contains terms that are proportional to such functions as $\exp(-\omega^2\sigma_{f1}^2)$, $\exp(-\omega^2\sigma_{f2}^2)$, and $\exp(-\omega^2(\sigma_{f1}^2+\sigma_{f2}^2)/2)$, and describe the oscillatory form of the background. The dispersions σ_{f1}^2 and σ_{f2}^2 characterize the smearing of the transition times and govern the rapidity of the decay of the background oscillations. Increasing the noise intensity leads to an increase in σ_{f1}^2 and σ_{f2}^2, i.e., an increase in the rapidity of the decay of the background oscillations.

For larger noise intensity (i.e., D comparable to the potential barrier height) the oscillatory form of the background disappears. This phenomenon occurs in the stochastic synchronization regime, characterized by the coincidence of an average switching frequency of the state point, with the driving frequency at the input [25]. This implies that the residence times are approximately one-half the period of the periodic force, i.e., the parameters $\alpha_p\simeq 1$ and $\alpha_q\simeq 1$, so that the expression for the background spectrum can be simplified as

$$Q_b(\omega)\simeq\frac{4X^2}{\pi T\omega^2}\left[1-\frac{1}{2}[\exp(-\omega^2\sigma_{f1}^2)+\exp(-\omega^2\sigma_{f2}^2)]\right].$$

In the low frequency regime, the last expression can be rewritten as

$$Q_b(\omega)\simeq\frac{4X^2}{\pi T\omega^2}\left[1-\frac{1}{2}(1-\omega^2\sigma_{f1}^2+1-\omega^2\sigma_{f2}^2)\right]$$
$$=\frac{4X^2}{\pi T}(\sigma_{f1}^2+\sigma_{f2}^2), \tag{66}$$

which coincides with the lower limit of the spectral background [see Eq. (58)]. Equation (66) shows that $Q_b(\omega)$ is proportional to the dispersion of the transition smearing and is independent of the frequency ω. The real background (see Fig. 5) depends on ω but varies very slowly.

4. Spectral background in the high frequency regime

In the high frequency limit, i.e., $\omega^2\sigma_{f1}^2\gg 1$ and $\omega^2\sigma_{f2}^2\gg 1$, we can assume that the exponential functions are zero, $\exp(-\omega^2\sigma_{f1}^2)\simeq 0$, $\exp(-\omega^2\sigma_{f2}^2)\simeq 0$, and $\exp(-\omega^2(\sigma_{f1}^2+\sigma_{f2}^2)/2)\simeq 0$. Then the expression (37) can be approximated as

$$Q_b(\omega)\simeq\frac{8X^2}{\pi T(\alpha_p+\alpha_q)\omega^2}, \tag{67}$$

i.e., the background density $Q_b(\omega)$ coincides with the average spectral background [see Eq. (50)]. The background $Q_b(\omega)$ is proportional to $1/\omega^2$, and decreases with growing frequency ω. It is easy to see that Eq. (67) is correct for weak and strong noise intensities.

C. Discussion

The expression (37) describes the spectral background and its peaks very well, however, it does not offer an insight into the origin of the peaks. Accordingly, in this section, we discuss the origin of these peaks. To this end, we first note an exact solution of the Eq. (4) that has been obtained in [10] wherein the general structure of the autocorrelation function and the power spectrum have been described.

In [10] it was shown that the autocorrelation function $\Psi(\tau)=\langle\langle y(t+\tau)y(t)\rangle\rangle$ (here the double brackets denote the ensemble and time averages) can be written as the sum $\Psi(\tau)=\Psi_p(\tau)+\Psi_b(\tau)$, where $\Psi_p(\tau)$ is a periodic function which corresponds to δ peaks in the power spectrum, and $\Psi_b(\tau)$ corresponds to the background of the power spectrum; it can be written in the form

$$\Psi_b(\tau)=e^{-\langle W\rangle|\tau|}\chi(\tau), \tag{68}$$

where $\langle W\rangle=T^{-1}\int_0^T[W_{12}(t)+W_{21}(t)]dt$ and $\chi(\tau)$ is a periodic function. Since the autocorrelation function must be symmetric, $\Psi(\tau)=\Psi(-\tau)$, the function $\chi(\tau)$ expanded in a Fourier series contains only cosines:

$$\chi(\tau)=\chi_0+\sum_{m=1}^{\infty}\chi_m\cos(m\Omega\tau). \tag{69}$$

The power spectrum can be found as the Fourier transform of the autocorrelation function, i.e., the background is $Q_b(\omega)=\int_0^\infty\Psi_b(\tau)\cos(\omega\tau)d\tau$. Using Eqs. (68) and (69), we obtain

$$Q_b(\omega)=\chi_0\frac{\langle W\rangle}{\langle W\rangle^2+\omega^2}+\sum_{m=1}^{\infty}\chi_m\left[\frac{\langle W\rangle}{\langle W\rangle^2+(m\Omega+\omega)^2}\right.$$
$$\left.+\frac{\langle W\rangle}{\langle W\rangle^2+(m\Omega-\omega)^2}\right]. \tag{70}$$

This result shows a structure of the spectral background that is consistent with the findings in Ref. [10]: The background is the sum of contributions centered at zero frequency, the drive frequency, and its harmonics. Unfortunately, a detailed analysis of Eq. (70) cannot be carried out because the coefficients χ_m cannot be found analytically in the strong forcing regime. However, for Eq. (70) to be consistent with the known properties of the spectral background it must follow that the coefficients χ_m with odd indexes m are positive and those with even indexes are negative. The positive coefficients correspond to the peaks and the negative coefficients correspond to the dips in the background. We emphasize that the peaks and dips are present (in the background) only in the strong forcing limit; this explains why they were not

predicted in [10] wherein only the weak forcing limit was considered.

We consider first the case of the symmetric potential, i.e., $c=0$. In [17] it has been shown that $\chi(\tau)$ contains only even nonzero harmonics, $\chi_{2m}\cos(2m\Omega\tau)$. This means that in the symmetric case the power spectrum background contains no peaks, but has dips only, in accordance with experiments [12] and previous analytical work [8,14].

In asymmetric case the odd harmonics of $\chi(\tau)$ are nonzero leading to the presence of peaks in the background. The peak height is proportional to χ_m [see Eq. (70)], but the widths of all the peaks (and dips) are approximately identical and proportional to $\langle W\rangle$.

IV. CONCLUSIONS

In this paper the analytic expression of the full power spectral density of the asymmetric two-state system driven by noise and a periodic (time-sinusoidal) force has been obtained. A detailed theoretical analysis of the PSD shows the following features.

(i) The following periodical alternation is seen in the peak heights in the PSD: At low frequencies, the odd harmonics have greater spectral amplitude than the even harmonics. With increasing frequency, a crossover occurs with the even harmonics having the greater spectral amplitudes, and with even higher frequency, another crossover occurs with the odd harmonics again having greater amplitude than the even ones, and so on.

(ii) At low frequencies, the power in the odd harmonics, Q_n, decreases as n^{-2}. In contrast to the odd harmonics, the power in the even harmonics is proportional to $(\delta_{f1}-\delta_{f2})^2$; they are quite weak, and disappear in the symmetric case, $c=0$.

(iii) In contrast to the monotonic dependence of the odd harmonics on the asymmetry c, the dependence of the even harmonics has a maximum.

(iv) In the limit of weak noise intensity the background contains dips that occur near even multiples of the driving frequency Ω. For the symmetric case ($c=0$) the minima of the dips coincide with even multiples of the driving frequency. When the system is rendered asymmetric ($c\neq 0$), however, the minima shift to the right on the frequency axis ($\omega_{\text{shift}}>0$) and it is linear dependent on n, i.e., the shift from the frequency 4 Ω is double the shift from 2 Ω.

(v) Finite width peaks arise in the spectral background of the asymmetric system only. The peaks are evident not only in the model with the two-state filter but also for the filterless model (see Fig. 10), i.e., the presence of the peaks in the power spectrum appears to be a general feature in nonlinear systems. For the asymmetric case, the peak maxima shift to the left ($\omega_{\text{shift}}<0$); the shift is proportional to n^{-1}, i.e., it decreases with increasing peak number. The dependence of the peak height on the asymmetry is nonmonotonic, and has a maximum. The peak height is proportional to n^{-2}, i.e., it decreases with increasing peak number.

(vi) All dips and peaks in the spectral background have the same width—this width is independent of the peak (or dip) number.

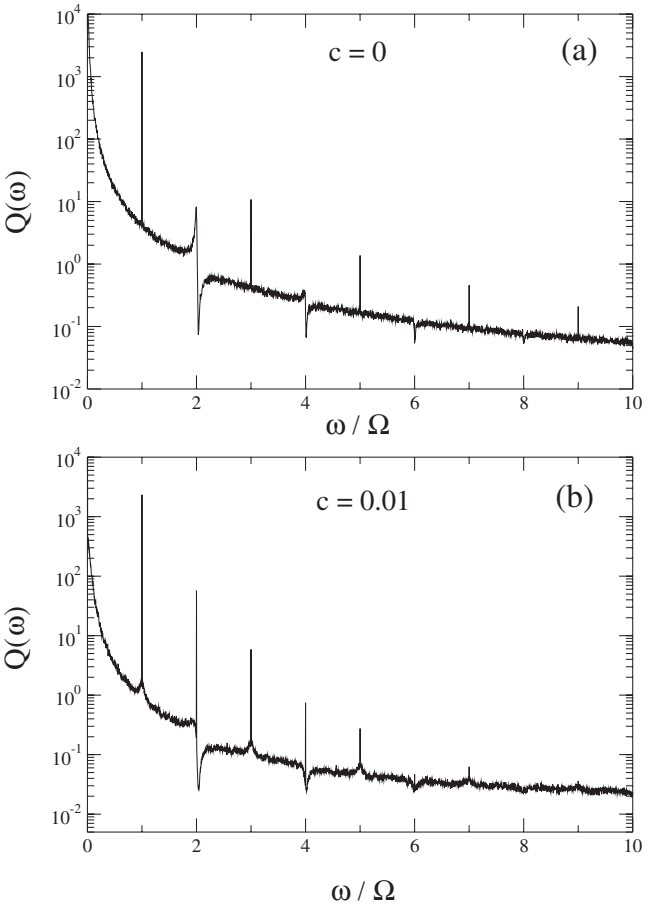

FIG. 10. The PSD for the parameters (a) $X=1.0$, $a=1.0$, $b=1.0$, $A=0.34$, $D=0.0015$, $\Omega=0.001$, $c=0.0$, and (b) $c=0.01$. The results were calculated by computer simulation of the model (1) without the use of the two-state filter (3).

(vii) The shift of the spectral minima, as well as the width of the dips and the peaks, increase with the asymmetry and noise intensity.

(viii) The depth of the dips monotonically decreases with growing asymmetry, but the dependence of the depth d on the noise intensity D is nonmonotonic, i.e., there is a maximum in d. This follows from the fact that, for weak noise intensity, the depth increases with noise, but the dips disappear for large noise intensity. One can show that the expression (50) is not a good estimate of the average of the spectral background for large noise intensity, i.e., the definition of the depth Eq. (51) in this case, has a small error. Clearly, a general calculation of the depth of the dips requires a more universal definition of the depth, and would be a subject for a future calculation.

The last point deserves some additional comment. For very small asymmetry the peaks in the spectral background are very narrow and only resolvable by an FFT having sufficient frequency resolution. This has implications for studies of stochastic resonance (SR), for example. Such studies often define the output signal-to-noise ratio (SNR) to be the integrated area of the fundamental spectral component to the integrated area of the spectral background. However, unless care is exercised, the peak in the spectral background will be

experimentally indistinguishable from the fundamental component (which, although theoretically a delta function, always has finite width set by the length of the observation). In turn, this could lead to a systematic overestimation of the SNR at small noise intensities and asymmetries, precisely the regime of interest for many real-world applications, e.g., weak magnetic field detection [18,19] and the detection of magnetic fields at nanometer scales [20] via occurrence of even harmonics of the periodic force [21].

We close this paper with a few sweeping comments. The results presented here, are valid for any form of the bistable potential, but they are calculated for a (binary) filtered output. They can be applied to any situation wherein the system is very strongly nonlinear i.e., the periodic signal amplitude is far greater than the noise intensity; in particular, they should apply to the case of a signal that is just barely subthreshold and also to one that is just barely suprathreshold (the situation of interest in some practical applications [19]). Hence they are not applicable to the (somewhat popular because of ease of calculation) linear response limit wherein the signal is very weak (usually subthreshold) and the noise relatively large.

Having obtained the response power spectral density, it is logical to enquire about the signal-to-noise ratio (SNR) measured at one of the peaks in the PSD. It can be shown that the SNR can be expressed in terms of six parameters of which four are obtained from the residence time distribution and the remaining two from the return times distribution [15]. We do not go into details here, preferring to leave the SNR to an upcoming paper.

ACKNOWLEDGMENTS

We gratefully acknowledge support from the US Office of Naval Research, Code 30.

APPENDIX A

We define the spectral density function via the finite Fourier transform [5],

$$Q(\omega) = \lim_{L\to\infty} \langle S_{yy}(\omega,L)\rangle, \tag{A1}$$

where the expectation value is denoted by the angular brackets, and the function $S_{yy}(\omega,L)$ is introduced:

$$S_{yy}(\omega,L) = \frac{1}{2\pi}\frac{1}{2L}\hat{y}_L^*(\omega)\hat{y}_L(\omega). \tag{A2}$$

Here, the hat denotes the Fourier transform which is taken over an interval of time $2L$,

$$\hat{y}_L(\omega) = \int_{-L}^{L} y(t)\exp(-i\omega t)dt. \tag{A3}$$

Equation (A2) can be rewritten in the following form:

$$\begin{aligned} S_{yy}(\omega,L) &= \frac{1}{2\pi}\frac{1}{2L}\int_{-L}^{L} y(t)e^{i\omega t}dt\int_{-L}^{L} y(\tau)e^{-i\omega\tau}d\tau \\ &= \frac{1}{2\pi}\frac{1}{2L}\int_{-L}^{L}\int_{-L}^{L} y(t)y(\tau)e^{-i\omega(\tau-t)}dt\,d\tau. \end{aligned} \tag{A4}$$

At this point, it is useful to introduce a new variable $\Lambda=\tau-t$, so that

$$\begin{aligned} S_{yy}(\omega,L) = &\frac{1}{2\pi}\int_{-2L}^{0}\left[\frac{1}{2L}\int_{-2\Lambda}^{2L} y(t)y(t+\Lambda)dt\right]e^{-i\omega\Lambda}d\Lambda \\ &+\frac{1}{2\pi}\int_{0}^{2L}\left[\frac{1}{2L}\int_{0}^{2L-2\Lambda} y(t)y(t+\Lambda)dt\right]e^{-i\omega\Lambda}d\Lambda. \end{aligned} \tag{A5}$$

Then, using the definition of the correlation function $R(t,\Lambda)=\langle y(t)y(t+\Lambda)\rangle$, we can write the following:

$$\begin{aligned} \langle S_{yy}(\omega,L)\rangle &= \frac{1}{2\pi}\int_{-2L}^{2L}\left[\frac{1}{2L}\int_{0}^{2L-2\Lambda} R(t,\Lambda)dt\right]e^{-i\omega\Lambda}d\Lambda \\ &= \frac{1}{2\pi}\int_{-2L}^{0}\left[\frac{1}{2L}\int_{-2\Lambda}^{0} R(t,\Lambda)dt\right]e^{-i\omega\Lambda}d\Lambda \\ &\quad+\frac{1}{2\pi}\int_{-2L}^{0}\left[\frac{1}{2L}\int_{2L-2\Lambda}^{2L} R(t,\Lambda)dt\right]e^{-i\omega\Lambda}d\Lambda. \end{aligned} \tag{A6}$$

Substituting Eq. (A6) into Eq. (A1) yields

$$Q(\omega) = \lim_{L\to\infty}\langle S_{yy}(\omega,L)\rangle = \frac{1}{2\pi}\int_{-\infty}^{\infty}\hat{R}(\Lambda)e^{-i\omega\Lambda}d\Lambda, \tag{A7}$$

where $\hat{R}(\Lambda)$ is the correlation function averaged over all values of time t. If the distribution of the stochastic process $y(t)$ is a periodic function of time, $P(y,t)=P(y,t+T)$, then the correlation function that can be calculated,

$$\hat{R}(\Lambda) = \frac{1}{T}\int_{0}^{T} R(t,\Lambda)dt,$$

is equivalent to an average of the correlation function over the initial phase ϕ of the periodic force, $A\cos(\Omega t+\phi)$.

APPENDIX B

The parameter p (introduced in Sec. II) can be approximated, in the weak noise limit, as

$$p = \exp(-I_1) = \sum_{n=0}^{\infty}\frac{(-I_1)^n}{n!} \simeq 1-I_1,$$

where $I_1=\sqrt{2\pi}W_{12\,\max}\delta t_1$ and $I_1 \ll 1$. Then, the parameter α_p is

$$\alpha_p = \frac{1+p}{1-p} \simeq \frac{2+I_1}{I_1} \simeq \frac{2}{I_1} = \frac{2}{\sqrt{2\pi}W_{12\,\max}\delta t_1}. \tag{B1}$$

Assuming $|\Delta x_0 c/D| \ll 1$ and using Eqs. (7)–(10), we can write

$$\alpha_p \simeq \frac{2\Omega\sqrt{2\pi|\Delta x_1|A}}{\sqrt{|V''_{xx}(x'_1,t')V''_{xx}(x'_{s1},t')|}\sqrt{D}}\exp\left(\frac{\Delta V_1}{D}\right) \simeq \frac{a_0}{\sqrt{D}}\exp\left(\frac{\Delta U_0}{D}\right)\left(1+\frac{\Delta x_0 c}{D}\right), \quad \text{(B2)}$$

where the time $t'=0$ corresponds to maximum of the periodic force, the parameters $x'_1=x_1(t')$ and $x'_{s1}=x_{s1}(t')$ are the locations of the minimum and maximum of the potential, the potential barrier is $\Delta V_1=V(x'_{s1},t')-V(x'_1,t')$, and $\Delta x_0 = \Delta x_1|_{c=0}=|x'_{s1}-x'_1|_{c=0}$, $\Delta U_0=\Delta V_1|_{c=0}$, $a_0 = 2\Omega\sqrt{2\pi|\Delta x_0|A/|V''_{xx}(x'_1,t')V''_{xx}(x'_{s1},t')|_{c=0}}$.

Similarly, the approximation of α_q for small c and D is

$$\alpha_q \simeq \frac{a_0}{\sqrt{D}}\exp\left(\frac{\Delta U_0}{D}\right)\left(1-\frac{\Delta x_0 c}{D}\right). \quad \text{(B3)}$$

From Eqs. (B2) and (B3) it follows that the difference $(\alpha_p-\alpha_q)$ is

$$\alpha_p-\alpha_q \simeq \frac{a_0}{\sqrt{D}}\exp\left(\frac{\Delta U_0}{D}\right)\frac{2\Delta x_0 c}{D}, \quad \text{(B4)}$$

which depends, linearly, on the asymmetry c. The sum $(\alpha_p+\alpha_q)$ is given by

$$\alpha_p+\alpha_q \simeq \frac{2a_0}{\sqrt{D}}\exp\left(\frac{\Delta U_0}{D}\right), \quad \text{(B5)}$$

which, in the limit of small c and D, is independent of the asymmetry c.

APPENDIX C

Using the approximations $\omega=n\Omega+\Delta\omega$ (where n is even), $\Delta\omega \ll n\Omega$, and $\sin(\omega T/2)=\sin(n\Omega T/2+\Delta\omega T/2) = \sin(\Delta\omega T/2)\simeq \Delta\omega T/2$, and $\cos(\omega T/2)\simeq 1$, $\omega\simeq n\Omega$, we can write the background (57) as

$$Q_b(n\Omega+\Delta\omega) \simeq \frac{8X^2}{\pi T(\alpha_p+\alpha_q)}\frac{1}{(n\Omega+\Delta\omega)^2} \times\left[1-\frac{[1-n^2\Omega^2(\sigma_{f1}^2+\sigma_{f2}^2)/2]}{\alpha_p^2\alpha_q^2\Delta\omega^2T^2/4+(\alpha_p+\alpha_q)^2} \times\{(\alpha_p+\alpha_q)^2+n\Omega(\alpha_p-\alpha_q)\alpha_p\alpha_q \times(\delta_{f1m}-\delta_{f2m})\Delta\omega T/2\}\right]. \quad \text{(C1)}$$

Then, assuming $(n\Omega+\Delta\omega)^2\simeq(n^2\Omega^2+2n\Omega\Delta\omega)$, $(1+2\Delta\omega/n\Omega)^{-1}\simeq(1-2\Delta\omega/n\Omega)$, and $[1+\alpha_p^2\alpha_q^2\Delta\omega^2T^2/4(\alpha_p+\alpha_q)^2]^{-1}\simeq[1-\alpha_p^2\alpha_q^2\Delta\omega^2T^2/4(\alpha_p+\alpha_q)^2]$, it is easy to obtain

$$Q_b(n\Omega+\Delta\omega) \simeq \frac{8X^2}{\pi T(\alpha_p+\alpha_q)}\frac{1}{(n^2\Omega^2+2n\Omega\Delta\omega)} \times\left[1-\frac{[1-n^2\Omega^2(\sigma_{f1}^2+\sigma_{f2}^2)/2]}{(\alpha_p+\alpha_q)^2} \times\frac{1}{1+\alpha_p^2\alpha_q^2\Delta\omega^2T^2/[4(\alpha_p+\alpha_q)^2]}\{(\alpha_p+\alpha_q)^2 +n\pi(\alpha_p-\alpha_q)\alpha_p\alpha_q(\delta_{f1m}-\delta_{f2m})\Delta\omega\}\right] \simeq \frac{8X^2}{\pi T(\alpha_p+\alpha_q)n^2\Omega^2}\left(1-\frac{2\Delta\omega}{n\Omega}\right) \times\left[1-\frac{[1-n^2\Omega^2(\sigma_{f1}^2+\sigma_{f2}^2)/2]}{(\alpha_p+\alpha_q)^2} \times\left(1-\frac{\alpha_p^2\alpha_q^2\Delta\omega^2T^2}{4(\alpha_p+\alpha_q)^2}\right)\{(\alpha_p+\alpha_q)^2 +n\pi(\alpha_p-\alpha_q)\alpha_p\alpha_q(\delta_{f1m}-\delta_{f2m})\Delta\omega\}\right] \quad \text{(C2)}$$

or

$$\begin{aligned} Q_b(n\Omega+\Delta\omega) &\simeq K_1(1-K_2\Delta\omega)[1-K_3(1-K_4\Delta\omega^2)\{K_5+K_6\Delta\omega\}] \\ &\simeq K_1(1-K_3K_5)+K_1(K_2K_3K_5-K_3K_6-K_2)\Delta\omega \\ &\quad +K_1(K_3K_4K_5+K_2K_3K_6)\Delta\omega^2 \\ &\quad +K_1(K_3K_4K_6-K_2K_3K_4K_5)\Delta\omega^3-K_1K_2K_3K_4K_6\Delta\omega^4. \end{aligned} \quad \text{(C3)}$$

Here, we have introduced the parameters

$$K_1=\frac{8X^2}{\pi T(\alpha_p+\alpha_q)n^2\Omega^2},$$

$$K_2=\frac{2}{n\Omega},$$

$$K_3=\frac{[1-n^2\Omega^2(\sigma_{f1}^2+\sigma_{f2}^2)/2]}{(\alpha_p+\alpha_q)^2},$$

$$K_4=\frac{\alpha_p^2\alpha_q^2T^2}{4(\alpha_p+\alpha_q)^2},$$

$$K_5=(\alpha_p+\alpha_q)^2,$$

$$K_6=n\pi(\alpha_p-\alpha_q)\alpha_p\alpha_q(\delta_{f1m}-\delta_{f2m}). \quad \text{(C4)}$$

The parabolic approximation can, then, be obtained by neglecting the terms with the small parameters $\Delta\omega^3$ and $\Delta\omega^4$ in Eq. (C3):

$$Q_b(\omega)=A_0+A_1(\omega-n\Omega)+A_2(\omega-n\Omega)^2, \quad \text{(C5)}$$

where we introduce the parameters

$$A_0=K_1(1-K_3K_5),$$

$$A_1=K_1(K_2K_3K_5-K_3K_6-K_2)\simeq -K_1K_3K_6,$$

$$A_2=K_1(K_3K_4K_5+K_2K_3K_6)\simeq K_1K_3K_4K_5. \quad \text{(C6)}$$

Then, the equation

$$Q_b(\omega)=Q_{\text{av}}(n\Omega) \quad \text{(C7)}$$

has the following solutions

$$\omega_{1,2} = n\Omega + \frac{-A_1 \pm \sqrt{A_1^2 - 4A_2(A_0 - K_1)}}{2A_2}$$
$$= n\Omega + \frac{K_6}{2K_4K_5} \pm \sqrt{\left(\frac{K_6}{2K_4K_5}\right)^2 + \frac{1}{K_4}}$$
$$\simeq n\Omega + \frac{K_6}{2K_4K_5} \pm \frac{1}{\sqrt{K_4}}, \tag{C8}$$

or

$$\omega_{1,2} = n\Omega + \frac{n\Omega^2}{2\pi}\frac{(\alpha_p - \alpha_q)(\delta_{f1m} - \delta_{f2m})}{\alpha_p\alpha_q} \pm \frac{\Omega}{\pi}\frac{\alpha_p + \alpha_q}{\alpha_p\alpha_q}. \tag{C9}$$

The width of the paraboloid is defined as

$$\Xi = |\omega_2 - \omega_1| = 2\frac{\Omega}{\pi}\frac{\alpha_p + \alpha_q}{\alpha_p\alpha_q}, \tag{C10}$$

and the minima of the dips can be found as the solution of the equation

$$\frac{dQ_b(\omega)}{d\omega} = 0, \tag{C11}$$

which, in the parabolic approximation, yields for the shift

$$\Delta\omega_{\min} = \frac{n\Omega^2}{2\pi}\frac{(\alpha_p - \alpha_q)(\delta_{f1m} - \delta_{f2m})}{\alpha_p\alpha_q}. \tag{C12}$$

Then, using Eqs. (B2)–(B4) and (48), we can rewrite the last expression as

$$\Delta\omega_{\min} = d_0\frac{c^2}{\sqrt{D}}\exp\left(-\frac{2\Delta U_0}{D}\right), \tag{C13}$$

in which d_0 is introduced as

$$d_0 = \frac{n|V''_{xx}(x'_1,t')V''_{xx}(x'_{s1},t')|\sqrt{\Delta x_0}}{2A\Omega\pi^2\sqrt{2\pi A}}. \tag{C14}$$

APPENDIX D

In the weak noise limit the value of $\Omega^2\sigma_{f1}^2$ becomes so small that $\Omega^2\sigma_{f1}^2 \ll 1$. Then, introducing the variable $\kappa = \Omega^2\sigma_{f1}^2$ we can write

$$\exp(n^2\varkappa) \simeq 1 + n^2\varkappa \tag{D1}$$

when n is small. Now we would like to estimate a minimal value $n_{\min 1}$ for which Eq. (D1) becomes invalid. By relaxing the condition (D1) we may write the new condition $n^2\kappa \leqslant 0.5$, i.e., $n_{\min 1}^2\kappa = 0.5$ corresponding to an approximation error less than 10%. Then we have

$$n_{\min 1} \simeq \frac{1}{\sqrt{2|\varkappa|}} = \frac{1}{\sqrt{2}\Omega\sigma_{f1}}. \tag{D2}$$

In [15] we found that

$$\sigma_{f1}^2 = \frac{\delta t_1^2}{1 + R_1^2}, \tag{D3}$$

where, in the weak noise limit the parameter $R_1 \simeq -W_{12\,\max}\delta t_1$. Making the substitutions Eq. (9) into Eq. (D3) and Eq. (D3) into Eq. (D2) we obtain

$$n_{\min 1} \simeq \left[|x_1(t) - x_s(t)|\frac{A}{2D} + \frac{W_{12\,\max}^2}{2\Omega^2}\right]^{1/2}, \tag{D4}$$

where $t = mT$ and m is an integer. We can readily obtain the analogous expression corresponding to the condition $\Omega^2\sigma_{f2}^2 \ll 1$,

$$n_{\min 2} \simeq \left[|x_2(t) - x_s(t)|\frac{A}{2D} + \frac{W_{21\,\max}^2}{2\Omega^2}\right]^{1/2}, \tag{D5}$$

where $t = (m + 0.5)T$.

Obviously, to obtain a critical number, n_c, for which the weak noise approach is valid we need to choose a minimal number from the set $\{n_{\min 1}, n_{\min 2}\}$, i.e.,

$$n_c = \min(n_{\min 1}, n_{\min 2}). \tag{D6}$$

Since $|\delta_{f1} - \delta_{f2}| < \sigma_{f1}$ and $|\delta_{f1} - \delta_{f2}| < \sigma_{f2}$, the following approximations are always valid:

$$\cos(n_c\Omega(\delta_{f1} - \delta_{f2})) \simeq 1 - n_c^2\Omega^2(\delta_{f1} - \delta_{f2})^2$$

and

$$\sin(n_c\Omega(\delta_{f1} - \delta_{f2})) \simeq n_c\Omega(\delta_{f1} - \delta_{f2}).$$

[1] For good overviews see, e.g., K. Wiesenfeld and F. Moss, Nature (London) **373**, 33 (1995); A. Bulsara and L. Gammaitoni, Phys. Today **49**(3), 39 (1996); L. Gammaitoni, P. Hänggi, P. Jung, and F. Marchesoni, Rev. Mod. Phys. **70**, 223 (1998); V. S. Anishchenko, A. B. Neiman, F. Moss, and L. Schimansky-Geier, Usp. Fiz. Nauk **169**, 7 (1999); [Phys. Usp. **42**, 7 (1999)].

[2] R. Benzi, A. Sutera, and A. Vilpiani, J. Phys. A **14**, L453 (1981); C. Nicolis, J. Stat. Phys. **70**, 3 (1993).

[3] A. Longtin, A. Bulsara, and F. Moss, Phys. Rev. Lett. **67**, 656 (1991) A. Longtin, A. Bulsara, D. Pierson, and F. Moss, Biol. Cybern. **70**, 569 (1994).

[4] P. Jung, Phys. Rep. **234**, 175 (1993).

[5] J. S. Bendat and A. G. Piersol, *Random data. Analysis and measurement procedures*, third ed. (Wiley, New York, 2000).

[6] B. McNamara and K. Wiesenfeld, Phys. Rev. A **39**, 4854 (1989).

[7] V. I. Melnikov, Phys. Rev. E **48**, 2481 (1993).

[8] N. G. Stocks, Nuovo Cimento Soc. Ital. Fis., D **17**, 925 (1995).

[9] R. F. Fox, Phys. Rev. A **39**, 4148 (1989).

[10] R. Löfstedt and S. N. Coppersmith, Phys. Rev. E **49**, 4821 (1994).

[11] T. Zhou and F. Moss, Phys. Rev. A **41**, 4255 (1990).
[12] L. B. Kiss, Z. Gingl, Z. Marton, J. Kertesz, F. Moss, G. Schmera, and A. Bulsara, J. Stat. Phys. **70**, 451 (1993).
[13] L. Gammaitoni, F. Marchesoni, E. Menichella-Saetta, and S. Santucci, Phys. Rev. E **51**, R3799 (1995).
[14] V. A. Shneidman, P. Jung, and P. Hänggi, Phys. Rev. Lett. **72**, 2682 (1994); V. A. Shneidman, P. Jung, and P. Hänggi, Europhys. Lett. **26**, 571 (1994).
[15] A. Nikitin, N. G. Stocks, and A. R. Bulsara, Phys. Rev. E **68**, 016103 (2003).
[16] A. Nikitin, N. G. Stocks, and A. R. Bulsara, Phys. Rev. E **68**, 036133 (2003).
[17] A. Nikitin, N. G. Stocks, and A. R. Bulsara, Phys. Lett. A **334**, 12 (2005).
[18] A. R. Bulsara, M. E. Inchiosa, and L. Gammaitoni, Phys. Rev. Lett. **77**, 2162 (1996); M. E. Inchiosa, A. R. Bulsara, and L. Gammaitoni, Phys. Rev. E **55**, 4049 (1997); L. Gammaitoni and A. R. Bulsara, Phys. Rev. Lett. **88**, 230601 (2002).
[19] A. R. Bulsara, C. Seberino, L. Gammaitoni, M. F. Karlsson, B. Lundqvist, and J. W. C. Robinson, Phys. Rev. E **67**, 016120 (2003).
[20] A. Grigorenko and P. Nikitin, IEEE Trans. Magn. **31**, 2491 (1995). A. Grigorenko, P. Nikitin, A. Slavin, and P. Zhou, J. Appl. Phys. **76**, 6335 (1994).
[21] F. Primdahl, J. Phys. E **12**, 241 (1979).
[22] R. I. Stratonovich, *Topics in the Theory of Random Noise*, Vol. 1 (Gordon and Breach, New York, 1963).
[23] N. G. van Kampen, *Stochastic processes in Physics and Chemistry* (North-Holland, Amsterdam, 1992).
[24] R. L. Badzey and P. Mohanty, Nature (London) **437**, 995 (2005).
[25] B. Shulgin, A. Neiman, and V. Anishchenko, Phys. Rev. Lett. **75**, 4157 (1995).